TÜBİTAK

Turkish Journal of Earth Sciences

http://journals.tubitak.gov.tr/earth/

Research Article

Turkish J Earth Sci
(2015) 24: 249-275
© TÜBİTAK
doi:10.3906/yer-1404-18

Nature and physicochemical conditions of crystallization in the South Dehgolan intrusion, NW Iran: mineral-chemical evidence

Fatemeh SARJOUGHIAN[1], Ali KANANIAN[2,*], David R. LENTZ[3], Jamshid AHMADIAN[4]

[1]Department of Earth Sciences, Faculty of Sciences, University of Kurdistan, Sanandaj, Iran
[2]School of Geology, College of Science, University of Tehran, Tehran, Iran
[3]Department of Earth Sciences, University of New Brunswick, Fredericton, New Brunswick, Canada
[4]Department of Geology, Payame Noor University, Tehran, Iran

Received: 25.04.2014 • **Accepted/Published Online:** 18.12.2014 • **Printed:** 29.05.2015

Abstract: The South Dehgolan intrusion in the Sanandaj-Sirjan Zone ranges in composition from calc-alkalic monzogabbro to syenite to alkalic granite. This suite is composed mainly of variable proportions of quartz, K-feldspar, plagioclase, biotite, hornblende, and pyroxene. The plagioclase composition varies between albite to labradorite. The biotites are Mg- to Fe-rich in the monzogabbro to granite, respectively. The amphiboles are calcic and the composition varies from magnesiohornblende to actinolite. Clinopyroxene compositions fall in the diopside-augite field. The average calculated near-solidus crystallization temperatures are 774 °C, 655 °C, and 775 °C for the monzogabbro-monzodiorite, syenite, and granite, respectively. Calculated average pressures of emplacement are 1.7, 1.3, and 1.9 kbar for the monzogabbro-monzodiorite, syenite, and granite rocks, respectively, crystallizing at different respective depths of about 6.7, 5.0, and 7.3 km. The interpreted oxygen fugacities in the monzogabbro-monzodiorite and syenite rocks are typical of arc magmas, with oxygen fugacities above the Ni-NiO buffer. Water contents in the monzogabbro-monzodiorite and syenite were calculated to range from 4.7 to 4.4 wt.% and in the granite is 3.8 wt.%. High water and volatile contents in the monzogabbro to syenite may have allowed the magma to reach shallower crustal levels. During the evolution of this magmatic system to higher silica contents, there was an increase in the activity of oxygen and decrease in the temperature and the emplacement depth from the monzogabbro-monzodiorite to syenite rocks; this is consistent with the typical evolution of the granitoid rocks. However, the calculated higher temperature and pressure and low fO_2 and H_2O content in the later granite reflects notable differences in its origin and crystallization conditions. The range in mineral compositions is this intrusive suite is consistent with a relationship to subduction of the Neotethys oceanic crust beneath the Central Iranian microcontinent, although there was a change from calc-alkaline to alkaline magmatism.

Key words: Thermobarometry, oxygen fugacity, South Dehgolan, Sanandaj-Sirjan Zone, Iran

1. Introduction

The South Dehgolan intrusion is hosted within the Sanandaj-Sirjan zone (SSZ) of northwestern Iran. The SSZ is the central terrane of the Zagros orogen (Alavi, 1994), which is situated between the Urumieh-Dokhtar magmatic arc and the Zagros fold-thrust belt that belongs to the 1500-km-long Zagros orogenic system. The SSZ (150–250 km wide) is one of the most complicated structural zones in Iran and consists of imbricated slices of metamorphosed and nonmetamorphosed Phanerozoic stratigraphic units of the Afro-Arabian passive continental margin and obducted ophiolites transported southwestward from the collisional Zagros suture zone towards interior parts of the Arabian craton (Alavi, 2004). Many parts of the SSZ, and especially the northern part, contain numerous plutons and a widespread Mesozoic volcanism (e.g., Mohajjel et al., 2003). The intrusive rocks are dominantly composed of granodiorites to granites with subordinate gabbros to tonalites, with different affinities, including I-, S-, and A-type granitoids. The various affinities that have been proposed for these intrusive rocks have led to some reinterpretation of the origin in the SSZ and related magmatism. Although there are many studies on the petrogenesis of this rock suite, the mineral chemistry and emplacement conditions of these rocks have not yet been fully evaluated.

The compositions of minerals provide a means of evaluating physicochemical conditions of magma during the emplacement of intrusive rocks. Determination of pressure and temperature of the various phases of this multiphase pluton has an important role in ascertaining its petrogenetic history within the context of regional

* Correspondence: kananian@khayam.ut.ac.ir

tectonism. Numerous studies have demonstrated that geobarometry is a useful tool for determining the depth of crystallization (e.g., Hammarstrom and Zen, 1986; Vyhnal et al., 1991; Schmidt, 1992; Anderson, 1996; Stein and Dietl, 2001). Knowledge of the depth of crystallization through to solidification of calc-alkaline plutons is critical to unraveling the complex chemical evolution of orogenic belts (Rutter et al., 1989) and provides indirect evidence for the ascent (or descent) of exposed crustal sections through time.

Oxygen fugacity (fO_2) is a convenient measure of oxidation state of melts, which is a critical parameter controlling magmatic processes (Kilinc et al., 1983; Kress and Carmichael, 1991; Ottonello et al., 2001; Botcharnikov et al., 2005); it influences the crystallization sequences of magmas, is reflected in the composition of crystallizing minerals (e.g., Elliott, 1998), affects the generation of different magma types (Carmichael, 1991), and influences physical and chemical properties of the magma, such as melt structure and viscosity (Jayasuriya et al., 2004) that may be used to understand petrogenesis.

The compositions of amphibole, biotite, and pyroxene are quite sensitive to variations in the composition of the magma and have a close relationship with their initial melt and can be used as a discriminating tool in identification of the nature and geodynamic setting of felsic to intermediate to mafic igneous rocks (e.g., Le Bas, 1962; Leterrier et al., 1982; Abdel-Rahman, 1994; Molina et al., 2009).

Chemical compositions of minerals in the South Dehgolan intrusive complex have not yet been determined, and so they were the focus of this study of examining compositions of these major rock-forming minerals. To estimate the conditions of crystallization of these magmatic rocks, pressure, temperature, oxygen fugacity, and content of water were calculated by applying various geothermobarometric methods to help constrain crystallization conditions, including depth of emplacement. Lastly, mineral-chemical systematics were used to discriminate the regional to local nature of the geotectonic setting of this intrusion and to correlate them with the thermotectonic changes in the SSZ.

2. Field characteristics

The South Dehgolan intrusion (35°4'N to 35°13'N, 47°16'E to 47°27'E), with an outcrop area of about 120 km^2 in northwestern Iran, is situated in the northeast SSZ. The surrounding rocks in the South Dehgolan intrusion are Jurassic andesite, rhyolite, and tuffs and Jurassic metasedimentary formations, including quartzites, shales, and limestones with a metamorphic aureole of skarn along with iron mineralization, which was developed around the intrusive rocks (Figure 1). The grade of contact metamorphism is low typically within the albite-epidote hornfels, but locally exhibits slightly higher temperatures up to the hornblende-hornfels facies.

The pluton is composed of a variety of petrographic types, including granite, syenite, and monzogabbro-monzodiorite. The age of the granitic rocks near the studied rocks, which intruded to sedimentary-volcanic rocks of the lower Jurassic, is estimated at 144 ± 2 to 149 ± 3 Ma by U–Pb zircon dating (Azizi et al., 2011); therefore, the studied intrusion is late Jurassic in age. The medium- to fine-grained monzogabbro-monzodiorite rocks in the eastern and northeastern margin of the pluton are generally dark gray to black in color. The light gray syenite is mainly medium- to fine-grained in the southeastern segment of the plutonic complex. Mafic microgranular enclaves are common in the syenites with a dioritic composition. Contact relations between the host rocks and the enclaves are generally sharp, rounded, or diffuse. The syenite rock bodies intruded the monzogabbro-monzodiorite rocks with sharp contact or locally have interaction zones with comingling-mixing features present.

The granitic rocks are undeformed and the most abundant rocks in the pluton have a medium- to fine-grained groundmass with a pinkish white color. Contacts between this unit with other units are intrusive and generally sharp. According to field observations, the existence of angular mafic xenoliths in the granites, and the occurrence of veining/diking of granitic material into the monzogabbro-monzodiorite rocks, it is clear that mafic rocks are generally older than felsic rocks.

3. Petrography

The classification of the South Dehgolan intrusion is shown on the QAP nomenclature diagram of Streckeisen (1976) based on modal mineral content. According to this nomenclature, monzogabbro-monzodiorite, syenite, and granite are the main rock types in the studied area (Figure 2).

3.1. Monzogabbroic-monzodioritic rocks

Monzogabbro-monzodiorite rocks are medium- to fine-grained and composed mainly of plagioclase, amphibole, and pyroxene with variable amounts of biotite, quartz, and orthoclase. Plagioclase occurs as euhedral to subhedral crystals and commonly shows oscillatory or normal concentric zoning and some of them are altered to epidote, calcite, sericite, and clay minerals. Plagioclase is locally mantled by orthoclase, forming an anti-rapakivi texture. Amphibole is the most abundant ferromagnesian mineral in the studied rocks, typically euhedral to subhedral, and rarely altered to chlorite, calcite, and epidote (Figure 3a). Pyroxene is subhedral to euhedral, in some samples locally replaced by actinolite, biotite, and chlorite. Petrographic studies suggest that pyroxene is the early phase in the sequence of crystallization. The biotite is highly pleochroic

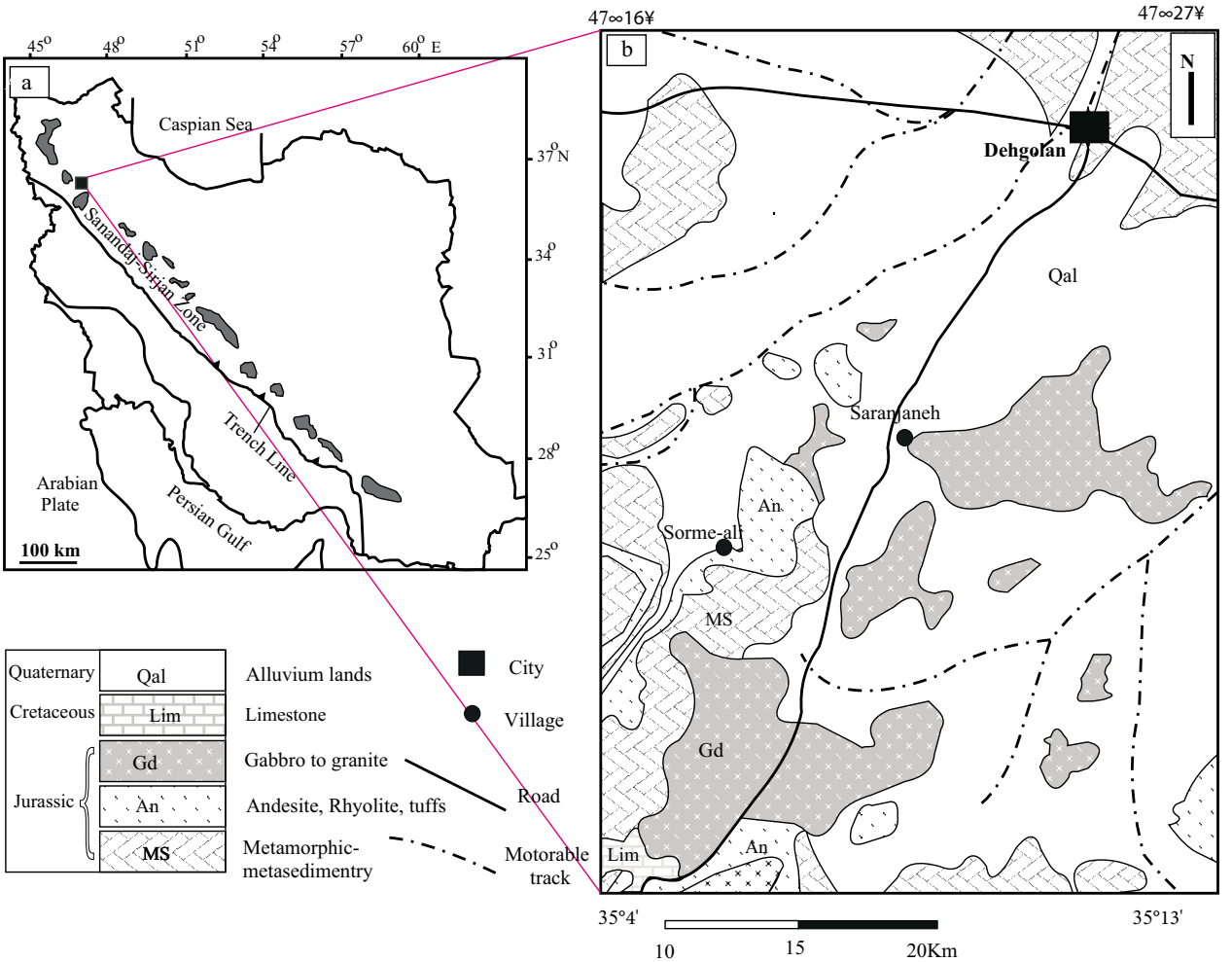

Figure 1. (a) Tectonic zones of the Zagros Orogenic belt of Iran and **(b)** geological map of the South Dehgolan intrusion, based on Zahedi et al. (1985; slightly modified).

in color and occurs as subhedral to anhedral crystals showing slight alteration to chlorite, titanite, and opaque minerals. K-feldspar grains are subhedral to anhedral with Carlsbad twinning without perthitic texture. They contain small inclusions of amphibole, biotite, plagioclase, and Fe–Ti oxides and locally show evidence of kaolinitization and sericitization. Quartz forms anhedral crystals with irregular boundaries and occupies the interstices between other minerals. Common accessory minerals are apatite, titanite, Fe–Ti-oxides, and rare epidote.

3.2. Syenitic rocks

Syenite is a medium- to fine-grained and composed of orthoclase, quartz, plagioclase, hornblende, biotite, pyroxene, and accessory minerals (mainly apatite, zircon, titanite, and opaque minerals). Orthoclase is the most abundant mineral, forming anhedral and subhedral crystals with small inclusions of other minerals (Figure 3b). In some samples, lamellae or patches of Na-rich feldspar exhibit a perthitic texture and are rarely replaced by kaolinite and sericite. Plagioclase crystals are euhedral to subhedral with polysynthetic twinning and are well zoned, and some samples are altered to sericite. Quartz is anhedral, fills interstices among other minerals, and generally shows undulatory extinction. Amphibole is the most abundant mafic phase with variable grain size. Amphibole is brownish green and has euhedral to subhedral habit. The brown biotite is pleochroic with subhedral to anhedral habits. They were formed late with respect to amphibole and early plagioclase, but they appear to have crystallized simultaneously with quartz, late plagioclase, and K-feldspar. Hornblende and biotite are slightly altered to chlorite, titanite, calcite, and opaque predominantly oxide minerals. Pyroxene has been observed in some samples and it is partially replaced with actinolite.

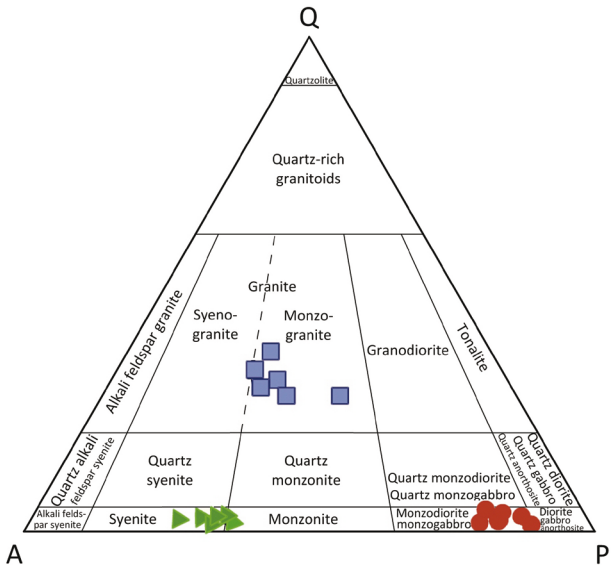

Figure 2. Classification of South Dehgolan intrusion according to modal mineralogy using the QAP diagram (Streckeisen, 1976). Circle: Monzogabbro-monzodiorite rocks, triangle: syenite rocks, square: granite rocks.

3.3. Granitic rocks

Granite is medium- to fine-grained with hypidiomorphic texture and is the main rock type in the area. It contains crystals of K-feldspar, quartz, plagioclase, and biotite with rare amphibole. K-feldspar is anhedral to subhedral and commonly shows perthitic texture and Carlsbad twins, and some of it contains euhedral inclusions of plagioclase and quartz grains. Quartz commonly occurs as anhedral grains clustered between orthoclase, plagioclase, and other quartz grains, but occasionally forms micrographic to granophyric intergrowths (Figure 3c). Plagioclase occurs as subhedral to euhedral crystals and is characterized by the common occurrence of lamellar twinning and oscillatory zoning. It is occasionally altered to sericite. The red-brown biotite and rare hornblende phenocrysts occur as discrete anhedral grains, as well as grain aggregates interstitial to feldspars and quartz, suggesting they are late-stage phases formed when water was concentrated. It is common that secondary chlorite, titanite, and opaque minerals replaced biotite minerals along their cleavage planes and margins. Accessory mineral phases are euhedral crystals of apatite, Fe–Ti oxides, and zircon.

4. Analytical methods

The mineral compositions of the South Dehgolan intrusion were determined by electron microprobe, with special emphasis on the biotite, feldspar, amphibole, and pyroxene. Several units of the South Dehgolan intrusion were sampled, and 10 of these samples were selected as representative of the different units of these plutons with minimal alteration evident.

At Naruto University, Japan, the EPMA (JEOL - JXA-8800R) was used with operating conditions of with 15 kV, 20 nA acceleration voltage, and 20 s counting time. We also used the CAMECA SX50 electron microprobe at the University of Oklahoma, USA, with five asynchronous wavelength-dispersive spectrometers and PGT PRISM 2000 energy-dispersive X-ray analyzer. Petrographic characterization was performed by backscattered electron imaging coupled with energy-dispersive X-ray analysis using a beam condition of 20 kV acceleration and 20 nA sample current. Chemical microanalysis was performed by wavelength-dispersive spectrometry using 20 kV acceleration, 20 nA beam current (measured at the Faraday cup), and 2 μm spot size. Matrix corrections employed the PAP algorithm (Pouchou and Pichoir, 1985), with oxygen content calculated by stoichiometry. Standard materials were natural crystalline solids for all elements, for which NIST glass K309 was used. Counting times were 30 s on peak for all elements, yielding minimum levels of detection (calculated at 3-δ above mean background) in the range of 0.01–0.02 wt.% of the oxides for all components, except Sr (0.04 wt.% SrO), Ba (0.09 wt.% BaO), and F (0.10 wt.% F).

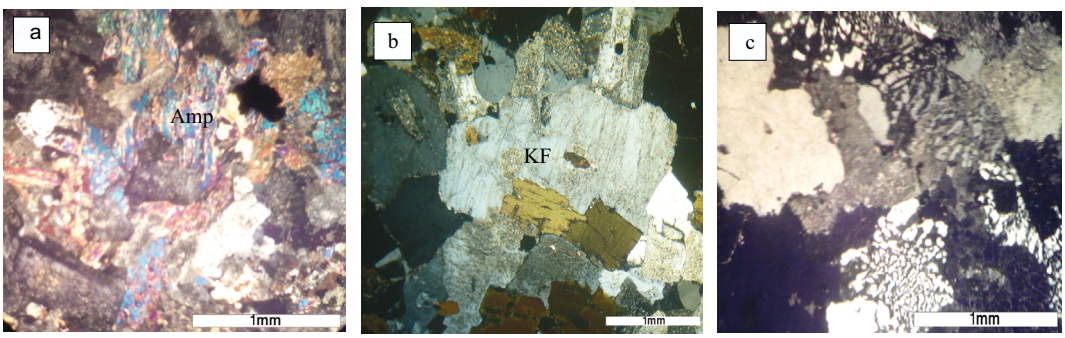

Figure 3. Photomicrographs (XPL) of mineral paragenesis: **(a)** abundant amphibole in the monzogabbro-monzodiorite, **(b)** K-feldspar crystals exhibit a perthitic texture intergrown with plagioclase and biotite in the syenite, **(c)** granophyric textures in the granite rocks.

Mineral recalculations were done using the Minpet Geological Software version 2.02 (Richard, 1995). Structural formulae of feldspars were calculated on the basis of 32 oxygens. Pyroxenes were classified by using the total numbers of specified cations at the M sites on the basis of 6 O atoms. The Fe^{3+} estimates were made using the general equation of Droop (1987) assuming 4 cations per formula unit. Formula calculations of amphibole were based on 23 atoms of oxygen, and their ferric/ferrous ratios were calculated by the charge balance method described by Robinson et al. (1982), using the average between the 15-NK and 13-CNK methods after applying the appropriate IMA site distribution rules (Leake et al., 1997). Biotite formulae were recalculated based on 24 O atoms and no OH groups.

5. Mineral compositions

5.1. Feldspar

Representative analyses of feldspar in the monzogabbro-monzodiorite, syenite, and granite are shown in Table 1. On the Ab–Or–An ternary diagram (Deer et al., 1992), plagioclase compositions in the granite and syenite rocks range from albite to oligoclase ($An_{3.6–12}$ and $An_{1–18.9}$) and in the monzogabbro-monzodiorite rocks range from oligoclase to labradorite ($An_{18–61}$). Plagioclase in the monzogabbro-monzodiorite exhibits oscillatory chemical zoning, whereas in the granites it shows normal zoning from An-rich cores to Ab-rich rims. Intraintrusion variation in the chemical composition of plagioclase may be interpreted by fractionation and/or the differences in sources, degrees of assimilation of wall rocks, and magmatic processes (see Yang and Lentz, 2005) and variation in the crystallization condition (Holton et al., 1999). Alkali-feldspar in granites corresponds to orthoclase with Or content between 72% and 97% (Figure 4). In the perthitic alkali feldspar, the potassic host phase is $Or_{97.7}Ab_{2.3}$ and the exsolved perthite is albite $Or_{0.9}Ab_{95.5}$.

5.2. Pyroxene

Electron microprobe analyses of pyroxene components are shown in Table 2. All of the pyroxenes in this area are Na-poor and their composition falls in the diopside-augite field according to the Morimoto's (1988) nomenclature (Figure 5). No significant differences are observed among clinopyroxene crystals from the monzogabbro-monzodiorite rocks, whereas those in the syenite samples are mainly Fe-rich diopside.

The analyzed pyroxene crystals are chemically heterogeneous and exhibit zoning as variations in parameters, such as Mg# [Mg/(Mg + Fe)], which are not systematic from core to rim, and rims are commonly more magnesian than cores. This may be related to changing physicochemical conditions through magma ascent. In fact, the composition of pyroxene depends not only on the melt composition, but also, albeit to a lesser extent, on the pressure, temperature, and volatile content during crystallization (see Davi et al., 2009). The Mg# of pyroxene decreases from the monzogabbros (average = 0.74) to the syenites (average = 0.50), and the average values show good correlation with the whole-rock compositions.

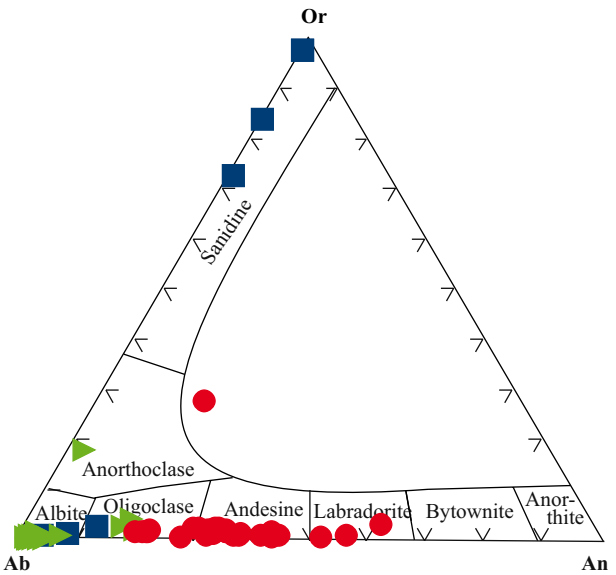

Figure 4. Compositions of feldspars of the South Dehgolan on the An–Ab–Or diagram (Deer et al., 1992); symbols as in Figure 2.

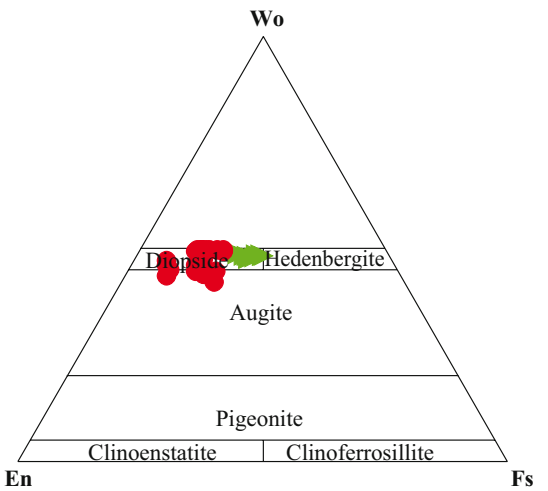

Figure 5. Wo-En-Fs ternary pyroxene classification diagram (Morimoto, 1988); symbols as in Figure 2.

Table 1. Electron microprobe analyses of feldspar in the South Dehgolan intrusion.

Sample	19A5.5	19A5.6	19A5.7	19A5.3	19A5.1	19A5.2	19A5.4	2C.3	2C.4.1	2C.4.2	2C.4.3	2C.5.1
Location	Gra	Gra	Gra	Gra	Gra	Gra	Gra	Syn	Syn	Syn	Syn	Syn
SiO_2	64.17	64.70	64.11	65.50	64.85	66.77	67.42	67.81	68.29	67.88	68.85	62.96
TiO_2	0.00	0.05	0.02	0.00	0.02	0.02	0.00	0.00	0.00	0.01	0.00	0.04
Al_2O_3	13.31	18.12	18.30	18.82	20.84	21.16	21.01	20.55	20.70	20.35	20.93	23.54
FeO	0.00	0.00	0.07	0.04	0.08	0.13	0.11	0.00	0.00	0.02	0.09	0.31
MnO	0.02	0.00	0.01	0.00	0.00	0.00	0.00	0.00	0.03	0.03	0.00	0.01
MgO	0.00	0.00	0.01	0.00	0.01	0.00	0.01	0.01	0.00	0.01	0.00	0.01
CaO	0.03	0.00	0.03	0.17	2.46	1.67	0.78	0.89	0.85	0.77	0.50	0.46
Na_2O	0.27	0.28	1.93	3.23	9.66	10.73	11.33	9.78	10.66	10.81	10.49	8.33
K_2O	17.82	17.92	15.44	13.33	0.51	0.27	0.15	0.09	0.03	0.09	0.26	2.87
Si	12.56	11.95	11.90	11.90	11.60	11.65	11.73	11.89	11.85	11.86	11.87	11.30
Al	3.07	3.94	4.00	4.03	4.39	4.35	4.30	4.24	4.23	4.19	4.25	4.98
Ti	0.00	0.01	0.00	0.00	0.00	0.00	0.00	0.00	0.00	0.00	0.00	0.01
Fe^{2+}	0.00	0.00	0.01	0.01	0.01	0.02	0.02	0.00	0.00	0.00	0.01	0.05
Mn	0.00	0.00	0.00	0.00	0.00	0.00	0.00	0.00	0.01	0.00	0.00	0.00
Mg	0.00	0.00	0.00	0.00	0.00	0.00	0.00	0.00	0.00	0.00	0.00	0.00
Ca	0.01	0.00	0.01	0.03	0.47	0.31	0.15	0.17	0.16	0.15	0.09	0.09
Na	0.10	0.10	0.70	1.14	3.35	3.63	3.82	3.33	3.59	3.66	3.51	2.90
K	4.45	4.22	3.66	3.09	0.12	0.06	0.03	0.02	0.01	0.02	0.06	0.66
Sum cations	20.18	20.22	20.27	20.19	19.93	20.02	20.05	19.65	19.83	19.88	19.78	19.98
Ab	2.2	2.3	16	26.7	85.1	90.7	95.5	94.6	95.6	95.7	95.9	79.5
An	0.1	0	0.2	0.8	12	7.8	3.6	4.8	4.2	3.8	2.5	2.4
Or	97.7	97.7	83.9	72.5	2.9	1.5	0.9	0.6	0.2	0.5	1.6	18

Syn: syenite; Gra: granite.

Table 1. (Continued).

Sample	2C.5.2	1B.11.1	1B.11.2	1B.11.3	1B.12.1	1B.12.2	1B.2.1	1B.2.2	1B.3.1	1B.3.2	1B.3.3	25A-1
Location	Syn	Syn	Syn	Syn	Syn	Syn	Syn	Syn	Syn	Syn	Syn	Syn
SiO_2	67.62	68.57	70.91	69.13	68.98	67.21	68.77	68.70	68.69	68.36	69.12	63.94
TiO_2	0.00	0.01	0.01	0.03	0.00	0.02	0.01	0.01	0.00	0.00	0.01	0.00
Al_2O_3	20.13	19.98	19.13	19.40	19.95	20.48	19.68	19.33	19.84	19.73	19.50	22.33
FeO	0.09	0.10	0.13	0.14	0.11	0.16	0.02	0.62	0.01	0.02	0.07	0.21
MnO	0.00	0.00	0.00	0.01	0.00	0.00	0.01	0.00	0.00	0.03	0.00	0.02
MgO	0.01	0.00	0.00	0.00	0.01	0.00	0.01	0.01	0.00	0.00	0.00	0.01
CaO	0.62	0.62	0.58	0.33	0.47	1.42	0.36	0.22	0.55	0.33	0.39	3.59
Na_2O	10.49	11.38	11.25	11.40	11.27	10.84	11.62	11.60	11.61	11.82	11.58	9.03
K_2O	0.05	0.09	0.10	0.19	0.15	0.17	0.05	0.10	0.05	0.06	0.05	0.71
Si	11.90	11.90	12.11	12.01	11.94	11.76	11.96	11.97	11.92	11.92	11.99	11.33
Al	4.17	4.09	3.85	3.97	4.07	4.22	4.03	3.97	4.06	4.05	3.98	4.66
Ti	0.00	0.00	0.00	0.00	0.00	0.00	0.00	0.00	0.00	0.00	0.00	0.00
Fe^{2+}	0.01	0.02	0.02	0.02	0.02	0.02	0.00	0.09	0.00	0.00	0.01	0.03
Mn	0.00	0.00	0.00	0.00	0.00	0.00	0.00	0.00	0.00	0.00	0.00	0.00
Mg	0.00	0.00	0.00	0.00	0.00	0.00	0.00	0.00	0.00	0.00	0.00	0.00
Ca	0.12	0.12	0.11	0.06	0.09	0.27	0.07	0.04	0.10	0.06	0.07	0.68
Na	3.58	3.83	3.73	3.84	3.78	3.68	3.92	3.92	3.91	4.00	3.90	3.10
K	0.01	0.02	0.02	0.04	0.03	0.04	0.01	0.02	0.01	0.01	0.01	0.16
Sum cations	19.80	19.97	19.83	19.94	19.93	19.98	19.99	20.01	20.00	20.05	19.96	19.97
Ab	96.5	96.6	96.7	97.4	96.9	92.4	98	98.4	97.2	98.2	97.9	78.70
An	3.2	2.9	2.8	1.5	2.2	6.7	1.7	1	2.5	1.5	1.8	17.30
Or	0.3	0.5	0.6	1.1	0.8	1	0.3	0.6	0.3	0.3	0.3	4.10

Syn: syenite.

Table 1. (Continued).

Sample	25A-2	25A-3	6A1.1	6A1.2	6A1.3	6A2.1	6A2.2	7B5.1	7B5.2	7B6.1	7B6.2
Location	Syn	Syn	Mg/Md	Mg/Md	Mg/Md	Mg/Md	Mg/Md	Mg/Md	Mg/Md	Mg/Md	Mg/Md
SiO_2	64.41	64.08	60.75	56.70	59.14	59.32	60.01	60.18	60.24	60.57	60.86
TiO_2	0.00	0.00	0.03	0.01	0.05	0.01	0.04	0.04	0.00	0.02	0.00
Al_2O_3	22.25	22.25	21.45	26.42	24.77	24.83	24.56	25.07	24.86	24.80	24.17
FeO	0.28	0.22	0.21	0.10	0.06	0.11	0.12	0.16	0.17	0.30	0.17
MnO	0.00	0.00	0.00	0.00	0.00	0.00	0.04	0.00	0.01	0.01	0.00
MgO	0.01	0.00	0.01	0.00	0.04	0.00	0.01	0.01	0.00	0.00	0.02
CaO	3.83	3.48	3.76	8.59	6.60	6.35	6.63	7.16	6.70	6.78	6.28
Na_2O	8.82	9.41	6.20	6.16	7.05	7.45	7.44	7.20	7.33	7.48	7.81
K_2O	0.38	0.51	4.82	0.27	0.39	0.19	0.37	0.33	0.45	0.32	0.39
Si	11.37	11.34	11.25	10.34	10.73	10.74	10.78	10.71	10.76	10.77	10.87
Al	4.63	4.64	4.68	5.67	5.29	5.29	5.19	5.26	5.23	5.19	5.08
Ti	0.00	0.00	0.00	0.00	0.01	0.00	0.01	0.01	0.00	0.00	0.00
Fe^{2+}	0.04	0.03	0.03	0.02	0.01	0.02	0.02	0.02	0.03	0.05	0.03
Mn	0.00	0.00	0.00	0.00	0.00	0.00	0.01	0.00	0.00	0.00	0.00
Mg	0.00	0.00	0.00	0.00	0.01	0.00	0.00	0.00	0.00	0.00	0.00
Ca	0.72	0.66	0.75	1.68	1.28	1.23	1.28	1.37	1.28	1.29	1.20
Na	3.02	3.23	2.23	2.18	2.48	2.62	2.59	2.49	2.54	2.58	2.71
K	0.09	0.12	1.14	0.06	0.09	0.04	0.09	0.08	0.10	0.07	0.09
Sum cations	19.87	20.01	20.08	19.94	19.90	19.94	19.95	19.93	19.94	19.95	19.98
Ab	78.80	80.60	54.1	55.6	64.4	67.2	65.6	63.3	64.7	65.4	67.7
An	18.90	16.50	18.1	42.8	33.3	31.7	32.3	34.8	32.7	32.8	30
Or	2.20	2.90	27.7	1.6	2.3	1.1	2.2	1.9	2.6	1.9	2.3

Syn: syenite, Mg/Md: monzogabbro/monzodiorite.

Table 1. (Continued).

Sample	7B6.3	14C.21.1	14C.21.2	14C.21.3	14C.21.4	7B.1.1	7B.1.2	7B.1.3	7B.2.1	7B.2.2	7B.2.3
Location	Mg/Md	Mg/Md	Mg/Md	Mg/Md	Mg/Md	Mg/Md	Mg/Md	Mg/Md	Mg/Md	Mg/Md	Mg/Md
SiO_2	59.59	54.00	58.59	63.70	58.81	59.08	59.24	63.08	62.58	63.28	63.23
TiO_2	0.02	0.04	0.06	0.06	0.04	0.07	0.06	0.04	0.06	0.03	0.06
Al_2O_3	24.31	28.73	25.67	22.68	25.52	25.24	25.21	22.99	22.74	23.04	22.80
FeO	0.16	0.29	0.29	0.27	0.26	0.16	0.18	0.24	0.16	0.26	0.17
MnO	0.01	0.01	0.01	0.02	0.00	0.00	0.01	0.00	0.00	0.00	0.00
MgO	0.00	0.00	0.02	0.00	0.00	0.01	0.00	0.00	0.00	0.00	0.00
CaO	6.49	11.48	7.85	4.10	7.78	7.34	7.29	4.53	4.39	4.52	4.32
Na_2O	7.55	4.90	7.06	9.41	7.04	7.31	7.27	8.92	8.91	8.99	9.11
K_2O	0.35	0.19	0.21	0.30	0.18	0.28	0.31	0.37	0.29	0.28	0.32
Si	10.79	9.80	10.51	11.23	10.56	10.61	10.63	11.16	11.18	11.17	11.20
Al	5.18	6.14	5.43	4.71	5.39	5.34	5.33	4.79	4.78	4.79	4.76
Ti	0.00	0.01	0.01	0.01	0.01	0.01	0.01	0.01	0.01	0.00	0.01
Fe^{2+}	0.03	0.04	0.04	0.04	0.04	0.02	0.03	0.04	0.02	0.04	0.03
Mn	0.00	0.00	0.00	0.00	0.00	0.00	0.00	0.00	0.00	0.00	0.00
Mg	0.00	0.00	0.01	0.00	0.00	0.00	0.00	0.00	0.00	0.00	0.00
Ca	1.26	2.23	1.51	0.77	1.50	1.41	1.40	0.86	0.84	0.86	0.82
Na	2.65	1.73	2.46	3.22	2.45	2.55	2.53	3.06	3.09	3.08	3.13
K	0.08	0.04	0.05	0.07	0.04	0.06	0.07	0.08	0.07	0.06	0.07
Sum cations	19.98	20.00	20.01	20.04	19.98	20.01	19.99	20.00	19.99	20.00	20.01
Ab	66.4	43.1	61.2	79.3	61.4	63.3	63.2	76.4	77.3	77	77.8
An	31.6	55.8	37.6	19.1	37.5	35.1	35	21.5	21	21.4	20.4
Or	2	1.1	1.2	1.7	1	1.6	1.8	2.1	1.7	1.6	1.8

Mg/Md: monzogabbro/monzodiorite.

Table 1. Continued.

Sample	7B.3.1	7B.3.2	7B.3.3	7B.5.1	7B.5.2	7B.5.3	8B.11.1	8B.11.2	8B.22.1	8B.22.2	8B.22.3
Location	Mg/Md	Mg/Md	Mg/Md	Mg/Md	Mg/Md	Mg/Md	Mg/Md	Mg/Md	Mg/Md	Mg/Md	Mg/Md
SiO_2	57.63	57.58	56.90	58.52	62.07	61.01	57.58	60.16	51.80	55.28	60.13
TiO_2	0.01	0.04	0.04	0.04	0.02	0.11	0.05	0.01	0.03	0.05	0.03
Al_2O_3	26.63	26.69	26.99	25.68	23.51	23.70	26.62	24.68	29.90	28.13	24.73
FeO	0.18	0.18	0.18	0.22	0.06	0.27	0.14	0.18	0.30	0.13	0.14
MnO	0.02	0.00	0.00	0.02	0.00	0.00	0.03	0.00	0.00	0.00	0.00
MgO	0.00	0.00	0.00	0.01	0.00	0.03	0.00	0.00	0.00	0.00	0.00
CaO	8.65	8.96	9.20	7.74	5.65	6.05	8.94	6.95	12.26	10.67	6.76
Na_2O	6.69	6.43	6.30	7.27	8.14	7.94	6.42	7.43	4.02	5.43	7.54
K_2O	0.20	0.23	0.16	0.19	0.09	0.42	0.10	0.33	0.51	0.13	0.25
Si	10.34	10.32	10.24	10.51	11.05	10.92	10.33	10.76	9.52	9.98	10.76
Al	5.63	5.63	5.72	5.43	4.93	5.00	5.63	5.20	6.47	5.98	5.21
Ti	0.00	0.01	0.01	0.01	0.00	0.02	0.01	0.00	0.00	0.01	0.00
Fe^{2+}	0.03	0.03	0.03	0.03	0.01	0.04	0.02	0.03	0.05	0.02	0.02
Mn	0.00	0.00	0.00	0.00	0.00	0.00	0.01	0.00	0.00	0.00	0.00
Mg	0.00	0.00	0.00	0.00	0.00	0.01	0.00	0.00	0.00	0.00	0.00
Ca	1.66	1.72	1.77	1.49	1.08	1.16	1.72	1.33	2.41	2.06	1.30
Na	2.33	2.24	2.20	2.53	2.81	2.76	2.23	2.58	1.43	1.90	2.62
K	0.05	0.05	0.04	0.04	0.02	0.10	0.02	0.08	0.12	0.03	0.06
Sum cations	20.03	19.99	20.00	20.05	19.89	19.99	19.97	19.96	20.01	19.98	19.96
Ab	57.7	55.7	54.8	62.3	71.9	68.7	56.2	64.7	36.1	47.6	65.9
An	41.2	42.9	44.2	36.6	27.6	28.9	43.2	33.4	60.9	51.7	32.7
Or	1.1	1.3	0.9	1.1	0.5	2.4	0.6	1.9	3	0.8	1.4

Mg/Md: monzogabbro/monzodiorite.

5.3. Amphibole

Representative electron microprobe analyses of amphibole in the monzogabbro-monzodiorite and syenite rocks are shown in Table 3. The amphiboles are considered to be members of the calcic amphibole family according to Leake's (1997) classification scheme, since they all show (Ca + Na) > 1.0 and $^{B}Na < 0.44$. A plot of the Si versus Mg/(Mg + Fe^{2+}) site and most of the amphiboles of the monzogabbro-monzosyenite and syenite rocks are magnesiohornblende to actinolite (Figure 6). Actinolitic hornblende and actinolite probably recrystallized as a subsolidus phase, since it falls outside the limits of igneous hornblende crystallization (Leake, 1971). Leake (1978) also suggested that amphiboles with Si > 7.3 are considered not to be magmatic, but rather a product of subsolidus reactions in the presence of an exsolved fluid (e.g., Chivas, 1981; Hendry et al., 1985; Agemar et al., 1999). Noticeably, some of the amphiboles in the syenites are ferrohornblendes. The Mg/(Mg + Fe) ratios of the amphiboles from the monzogabbro-monzodiorite are slightly higher (average = 0.53) than those observed in the syenite (average = 0.40).

5.4. Biotite

Electron microprobe analyses of biotite components from the studied intrusion are shown in Table 4. In all analyzed samples, biotite is fresh with minimal alteration effects (Figure 7a; Nachit et al., 2005). According to the revised mica classification (Rieder et al., 1999), all of the studied biotites plot in the biotite field, and its compositions in the granite and some monzodiorite rocks, show a slight tendency toward iron enrichment (Figure 7b).

Most of the biotite analyzed are Mg-rich in the monzogabbro (average X_{Mg} = 0.55) to Fe-rich in the granite rocks (average X_{Mg} = 0.28). Biotite analyses from the monzogabbro have higher SiO_2 contents and X_{Mg} values, with lower FeO relative to biotite from the granite.

6. Discussion

6.1. Crystallization conditions

6.1.1. Thermobarometry

Al-in-hornblende barometry has been widely used to calculate pressures of magmatic crystallization and to constrain the emplacement depths of batholiths (e.g., Anderson and Smith, 1995; Stein and Dietl, 2001; Ernst, 2002), although the computed pressure may reflect the level at which the hornblende crystallizes rather than the pressure at which the granitic rock consolidates (Ague, 1997). Therefore, Al-hornblende barometry must be used only in the presence of suitable mineral assemblages in granitoid rocks (quartz + plagioclase + alkali feldspar +

Table 2. Electron microprobe analyses of pyroxene in the South Dehgolan intrusion.

Sample	2C.2.1	2C.2.2	2C.4.1	2C.4.2	2C.5.1	2C.5.1	2C.5.2	25A.1	25A.2	25A.3	25A.5	25A.6
Location	Syn	Syn	Syn	Syn	Syn	Syn	Syn	Syn	Syn	Syn	Syn	Syn
SiO_2	51.88	51.85	51.42	51.89	51.02	51.76	51.84	52.97	53.05	52.33	52.78	52.76
TiO_2	0.00	0.08	0.05	0.00	0.12	0.10	0.02	0.01	0.03	0.03	0.00	0.00
Al_2O_3	0.13	0.25	0.27	0.12	0.32	0.37	0.25	0.18	0.27	0.15	0.20	0.18
FeO	14.31	15.42	15.09	13.93	14.96	14.52	15.02	11.80	12.26	14.44	13.47	13.07
Cr_2O_3	0.01	0.02	0.00	0.01	0.05	0.00	0.02	0.00	0.00	0.00	0.00	0.00
MnO	0.36	0.36	0.41	0.41	0.40	0.40	0.29	0.27	0.33	0.37	0.36	0.43
NiO	0.02	0.04	0.04	0.01	0.00	0.00	0.00	0.00	0.00	0.00	0.01	0.00
MgO	9.82	8.84	8.73	10.23	8.91	9.51	8.78	10.69	10.65	9.24	9.97	10.30
CaO	23.17	23.11	22.70	23.13	23.17	23.05	22.73	23.63	23.50	23.38	23.02	23.27
Na_2O	0.26	0.34	0.33	0.35	0.49	0.36	0.48	0.26	0.34	0.37	0.38	0.28
K_2O	0.03	0.00	0.01	0.00	0.00	0.00	0.01	0.00	0.00	0.00	0.01	0.00
T site												
Si	1.99	1.99	2.00	1.98	1.97	1.99	2.01	2.02	2.01	2.00	2.01	2.01
Al	0.01	0.01	0.00	0.01	0.02	0.02	0.00	0.00	0.00	0.00	0.00	0.00
Fe^{3+}	0.01	0.00	0.00	0.01	0.01	0.00	0.00	0.00	0.00	0.00	0.00	0.00
M1 site												
Al	0.00	0.00	0.01	0.00	0.00	0.00	0.01	0.01	0.01	0.01	0.01	0.01
Ti	0.00	0.00	0.00	0.00	0.00	0.00	0.00	0.00	0.00	0.00	0.00	0.00
Fe^{3+}	0.03	0.02	0.01	0.05	0.06	0.04	0.01	0.00	0.00	0.01	0.00	0.00
Fe^{2+}	0.41	0.46	0.47	0.37	0.42	0.42	0.47	0.38	0.39	0.45	0.42	0.41
Cr	0.00	0.00	0.00	0.00	0.00	0.00	0.00	0.00	0.00	0.00	0.00	0.00
Mg	0.56	0.51	0.51	0.58	0.51	0.54	0.51	0.61	0.60	0.53	0.57	0.58
Ni	0.00	0.00	0.00	0.00	0.00	0.00	0.00	0.00	0.00	0.00	0.00	0.00
M2 site												
Mg	0.00	0.00	0.00	0.00	0.00	0.00	0.00	0.00	0.00	0.00	0.00	0.00
Fe^{2+}	0.02	0.01	0.01	0.01	0.00	0.01	0.01	0.00	0.00	0.00	0.01	0.01
Mn	0.01	0.01	0.01	0.01	0.01	0.01	0.01	0.01	0.01	0.01	0.01	0.01
Ca	0.95	0.95	0.95	0.95	0.96	0.95	0.94	0.96	0.95	0.96	0.94	0.95
Na	0.02	0.03	0.03	0.03	0.04	0.03	0.04	0.02	0.03	0.03	0.03	0.02
K	0.00	0.00	0.00	0.00	0.00	0.00	0.00	0.00	0.00	0.00	0.00	0.00
Sum cations	4.00	4.00	4.00	4.00	4.00	4.00	4.00	4.00	4.00	4.00	4.00	4.00
Wo	48.00	48.41	48.35	47.64	48.72	48.09	48.47	49.31	48.80	48.90	48.27	48.34
En	28.29	25.78	25.88	29.30	26.07	27.60	26.05	31.03	30.78	26.91	29.10	29.77
Fs	23.71	25.81	25.77	23.06	25.22	24.30	25.48	19.67	20.42	24.19	22.64	21.90
Mg#	0.55	0.51	0.51	0.57	0.52	0.54	0.51	0.62	0.61	0.53	0.57	0.58

Syn: syenite.

Table 2. Continued.

Sample	6A.7.1	6A.7.2	6A.7.3	6A.7.4	7B.4.3	7B.4.4	7B.4.5	4C.2.1	4C.2.2	4C.2.3	9C.1.1	9C.1.2
Location	Mg/Md	Mg/Md	Mg/Md	Mg/Md	Mg/Md	Mg/Md	Mg/Md	Mg/Md	Mg/Md	Mg/Md	Mg/Md	Mg/Md
SiO_2	53.94	52.34	54.25	52.42	52.17	51.33	52.39	53.45	53.68	53.76	53.16	53.60
TiO_2	0.16	0.49	0.14	0.75	0.29	0.49	0.34	0.10	0.09	0.04	0.00	0.07
Al_2O_3	0.51	2.06	1.00	2.49	1.47	2.45	1.42	0.51	0.19	0.16	0.23	0.37
FeO	4.28	5.33	4.57	5.15	11.05	11.20	9.71	8.44	8.72	8.28	10.55	8.02
Cr_2O_3	0.17	0.51	0.28	0.16	0.12	0.01	0.03	0.02	0.01	0.02	0.01	0.01
MnO	0.14	0.10	0.14	0.10	0.40	0.39	0.37	0.32	0.32	0.30	0.32	0.27
NiO	0.09	0.00	0.06	0.00	0.00	0.00	0.07	0.00	0.00	0.00	0.01	0.00
MgO	16.90	16.88	16.64	16.30	13.29	13.33	14.12	14.05	13.56	13.82	11.62	13.21
CaO	24.21	21.60	22.89	21.95	22.14	20.17	22.30	23.06	23.48	23.39	24.34	24.66
Na_2O	0.08	0.27	0.25	0.22	0.32	0.54	0.33	0.15	0.16	0.11	0.04	0.01
K_2O	0.00	0.00	0.00	0.02	0.06	0.17	0.04	0.00	0.01	0.00	0.00	0.00
T site												
Si	1.96	1.92	1.98	1.93	1.93	1.92	1.93	1.99	2.00	2.01	2.01	2.00
Al	0.02	0.08	0.02	0.07	0.06	0.08	0.06	0.01	0.00	0.00	0.00	0.00
Fe^{3+}	0.01	0.00	0.00	0.00	0.00	0.00	0.01	0.00	0.00	0.00	0.00	0.00
M1 site												
Al	0.00	0.01	0.02	0.04	0.00	0.03	0.00	0.01	0.01	0.01	0.01	0.02
Ti	0.00	0.01	0.00	0.02	0.01	0.01	0.01	0.00	0.00	0.00	0.00	0.00
Fe^{3+}	0.03	0.04	0.00	0.00	0.07	0.07	0.07	0.00	0.00	0.00	0.00	0.00
Fe^{2+}	0.04	0.00	0.06	0.04	0.18	0.14	0.14	0.20	0.24	0.22	0.33	0.25
Cr	0.01	0.02	0.01	0.01	0.00	0.00	0.00	0.00	0.00	0.00	0.00	0.00
Mg	0.92	0.92	0.91	0.89	0.73	0.74	0.78	0.78	0.75	0.77	0.65	0.74
Ni	0.00	0.00	0.00	0.00	0.00	0.00	0.00	0.00	0.00	0.00	0.00	0.00
M2 site												
Mg	0.00	0.01	0.00	0.00	0.00	0.00	0.00	0.00	0.00	0.00	0.00	0.00
Fe^{2+}	0.05	0.12	0.08	0.12	0.08	0.13	0.08	0.06	0.04	0.04	0.00	0.00
Mn	0.00	0.00	0.00	0.00	0.01	0.01	0.01	0.01	0.01	0.01	0.01	0.01
Ca	0.95	0.85	0.90	0.87	0.88	0.81	0.88	0.92	0.94	0.94	0.98	0.99
Na	0.01	0.02	0.02	0.02	0.02	0.04	0.02	0.01	0.01	0.01	0.00	0.00
K	0.00	0.00	0.00	0.00	0.00	0.01	0.00	0.00	0.00	0.00	0.00	0.00
Sum cations	4.00	4.00	4.00	4.00	4.00	3.99	4.00	4.00	4.00	4.00	4.00	4.00
Wo	47.31	43.79	46.04	45.05	44.66	42.22	44.77	46.63	47.52	47.43	49.68	49.80
En	45.94	47.61	46.57	46.54	37.30	38.83	39.44	39.53	38.19	38.99	33.00	37.12
Fs	6.75	8.59	7.40	8.41	18.04	18.95	15.79	13.83	14.29	13.59	17.32	13.07
Mg#	0.88	0.85	0.87	0.85	0.68	0.68	0.72	0.75	0.73	0.75	0.66	0.75

Mg/Md: monzogabbro/monzodiorite.

Table 2. Continued.

Sample	9C.1.3	9C.1.4	9C.1.1	9C.1.2	9C.2.1	9C.2.2	9C.2.3	9C.3.1	9C.3.2	9C.3.3	8B.2.1	8B.2.2	8B.2.3
Location	Mg/Md	Mg/Md	Mg/Md	Mg/Md	Mg/Md	Mg/Md	Mg/Md	Mg/Md	Mg/Md	Mg/Md	Mg/Md	Mg/Md	Mg/Md
SiO_2	53.38	53.88	53.63	53.87	53.13	53.51	53.30	53.25	53.32	52.72	53.86	53.53	54.22
TiO_2	0.06	0.05	0.06	0.02	0.02	0.08	0.02	0.00	0.07	0.00	0.11	0.06	0.11
Al_2O_3	0.69	0.48	0.49	0.17	0.23	0.75	0.35	0.39	0.42	0.26	0.50	0.31	0.50
FeO	7.73	7.79	7.83	7.18	9.65	7.21	8.82	8.35	8.49	10.38	9.62	8.13	8.59
Cr_2O_3	0.00	0.00	0.00	0.00	0.00	0.00	0.00	0.00	0.01	0.02	0.01	0.02	0.00
MnO	0.23	0.25	0.21	0.42	0.33	0.18	0.29	0.23	0.28	0.33	0.33	0.29	0.26
NiO	0.00	0.02	0.01	0.02	0.00	0.00	0.00	0.01	0.01	0.00	0.00	0.00	0.02
MgO	13.52	13.49	13.38	13.79	12.13	13.86	12.77	12.99	13.19	11.70	14.21	14.40	14.70
CaO	24.90	24.63	24.76	24.85	24.52	24.61	24.58	24.73	24.42	24.11	21.81	22.98	22.09
Na_2O	0.03	0.03	0.04	0.00	0.02	0.04	0.05	0.04	0.03	0.03	0.22	0.14	0.20
K_2O	0.00	0.00	0.00	0.01	0.01	0.00	0.00	0.01	0.01	0.00	0.00	0.00	0.02
T site													
Si	1.98	2.00	2.00	2.00	2.00	1.99	2.00	1.99	1.99	2.00	2.00	1.99	2.00
Al	0.02	0.00	0.01	0.00	0.00	0.01	0.00	0.01	0.01	0.00	0.00	0.01	0.00
Fe^{3+}	0.00	0.00	0.00	0.00	0.00	0.00	0.00	0.00	0.00	0.00	0.00	0.00	0.00
M1 site													
Al	0.01	0.02	0.02	0.01	0.01	0.02	0.01	0.01	0.01	0.01	0.02	0.01	0.02
Ti	0.00	0.00	0.00	0.00	0.00	0.00	0.00	0.00	0.00	0.00	0.00	0.00	0.00
Fe^{3+}	0.01	0.00	0.00	0.00	0.00	0.00	0.00	0.00	0.00	0.00	0.00	0.00	0.00
Fe^{2+}	0.23	0.23	0.24	0.22	0.30	0.21	0.28	0.26	0.25	0.33	0.19	0.19	0.17
Cr	0.00	0.00	0.00	0.00	0.00	0.00	0.00	0.00	0.00	0.00	0.00	0.00	0.00
Mg	0.75	0.75	0.74	0.76	0.68	0.77	0.71	0.73	0.73	0.66	0.79	0.80	0.81
Ni	0.00	0.00	0.00	0.00	0.00	0.00	0.00	0.00	0.00	0.00	0.00	0.00	0.00
M2 site													
Mg	0.00	0.00	0.00	0.00	0.00	0.00	0.00	0.00	0.00	0.00	0.00	0.00	0.00
Fe^{2+}	0.00	0.01	0.00	0.00	0.00	0.01	0.00	0.00	0.01	0.00	0.11	0.06	0.10
Mn	0.01	0.01	0.01	0.01	0.01	0.01	0.01	0.01	0.01	0.01	0.01	0.01	0.01
Ca	0.99	0.98	0.99	0.99	0.99	0.98	0.99	0.99	0.98	0.98	0.87	0.92	0.87
Na	0.00	0.00	0.00	0.00	0.00	0.00	0.00	0.00	0.00	0.00	0.02	0.01	0.01
K	0.00	0.00	0.00	0.00	0.00	0.00	0.00	0.00	0.00	0.00	0.00	0.00	0.00
Sum cations	4.00	4.00	4.00	4.00	4.00	4.00	4.00	4.00	4.00	4.00	4.00	4.00	4.00
Wo	49.87	49.58	49.87	49.73	49.85	49.55	49.70	49.96	49.21	49.45	44.19	46.34	44.67
En	37.68	37.78	37.49	38.40	34.31	38.83	35.92	36.51	36.99	33.39	40.06	40.40	41.36
Fs	12.45	12.64	12.64	11.88	15.84	11.62	14.38	13.53	13.80	17.15	15.74	13.26	13.97
Mg#	0.76	0.76	0.75	0.77	0.69	0.77	0.72	0.74	0.73	0.67	0.73	0.76	0.75

Mg/Md: monzogabbro/monzodiorite.

Table 3. Electron microprobe analyses of amphibole in the South Dehgolan intrusion.

Sample	6A3.1	6A3.2	6A3.3	6A6.1	6A6.2	8B.21	8B.22	8B.23	8B.32.1	8B.32.2	8B.32.3
Location	Mg/Md	Mg/Md	Mg/Md	Mg/Md	Mg/Md	Mg/Md	Mg/Md	Mg/Md	Mg/Md	Mg/Md	Mg/Md
SiO_2	50.13	50.64	50.15	50.24	49.98	43.84	45.12	43.46	44.71	44.93	43.42
TiO_2	0.54	0.48	0.85	0.80	1.04	2.35	2.11	2.10	2.14	2.12	2.36
Al_2O_3	3.31	2.76	3.88	3.60	4.50	9.68	8.91	9.59	9.06	8.93	9.58
FeO	17.21	17.16	18.90	17.88	18.05	15.06	14.49	15.16	14.92	14.72	15.61
Cr_2O_3	0.03	0.01	0.00	0.02	0.02	0.06	0.05	0.05	0.03	0.01	0.04
MnO	0.40	0.33	0.54	0.50	0.43	0.22	0.17	0.22	0.20	0.18	0.21
MgO	11.79	13.34	11.95	12.34	12.38	11.97	12.56	12.26	12.64	12.68	11.70
CaO	11.89	10.93	9.66	10.77	10.93	11.32	11.62	10.90	11.35	11.14	11.32
Na_2O	0.28	0.41	0.56	0.63	0.86	1.79	1.65	1.75	1.73	1.75	1.80
K_2O	0.26	0.22	0.28	0.27	0.29	0.94	0.86	0.93	0.87	0.81	0.96
T site											
Si	7.51	7.42	7.29	7.35	7.22	6.50	6.65	6.46	6.57	6.61	6.47
Al	0.49	0.48	0.66	0.62	0.77	1.50	1.35	1.54	1.43	1.39	1.53
Fe^{3+}	0.00	0.11	0.05	0.03	0.02	0.00	0.00	0.00	0.00	0.00	0.00
C site											
Al	0.10	0.00	0.00	0.00	0.00	0.19	0.20	0.13	0.14	0.15	0.16
Cr	0.00	0.00	0.00	0.00	0.00	0.01	0.01	0.01	0.00	0.00	0.01
Fe^3	0.32	0.89	1.30	0.87	0.88	0.49	0.38	0.79	0.59	0.61	0.52
Ti	0.06	0.05	0.09	0.09	0.11	0.26	0.23	0.24	0.24	0.23	0.27
Mg	2.63	2.91	2.59	2.69	2.67	2.65	2.76	2.72	2.77	2.78	2.60
Fe^{2+}	1.83	1.10	0.95	1.29	1.29	1.38	1.40	1.10	1.24	1.20	1.43
Mn	0.05	0.04	0.07	0.06	0.05	0.03	0.02	0.03	0.03	0.02	0.03
B site											
Ca	1.91	1.72	1.51	1.69	1.69	1.80	1.83	1.74	1.79	1.76	1.81
Na	0.08	0.12	0.16	0.18	0.24	0.20	0.17	0.27	0.21	0.25	0.19
A site											
Na	0.00	0.00	0.00	0.00	0.00	0.31	0.31	0.24	0.28	0.25	0.33
K	0.05	0.04	0.05	0.05	0.05	0.18	0.16	0.18	0.16	0.15	0.18
Sum cations	15.04	14.87	14.72	14.92	14.99	15.49	15.47	15.42	15.44	15.41	15.51
Fe#	0.45	0.42	0.47	0.45	0.45	0.41	0.39	0.41	0.40	0.39	0.43
Mg#	0.55	0.58	0.53	0.55	0.55	0.59	0.61	0.59	0.60	0.61	0.57

Mg/Md: monzogabbro/monzodiorite.

Table 3. (Continued).

Sample	8B.32.4	8B.431	8B.432	8B.433	8B.434	7B1.1	7B1.2	7B2.1	7B2.2	7B.11	7B.12
Location	Mg/Md	Mg/Md	Mg/Md	Mg/Md	Mg/Md	Mg/Md	Mg/Md	Mg/Md	Mg/Md	Mg/Md	Mg/Md
SiO_2	51.92	45.21	44.48	44.29	55.71	47.14	47.21	46.48	46.37	50.42	46.45
TiO_2	0.26	2.17	2.36	2.38	0.06	1.34	1.45	1.70	1.73	0.29	0.62
Al_2O_3	4.34	8.99	9.10	9.27	0.63	6.88	6.78	7.08	6.72	3.01	5.87
FeO	12.21	14.87	14.95	14.75	11.57	16.59	16.89	16.64	17.39	22.58	23.01
Cr_2O_3	0.00	0.05	0.04	0.07	0.03	0.02	0.04	0.02	0.00	0.02	0.01
MnO	0.22	0.17	0.18	0.16	0.22	0.26	0.34	0.29	0.31	0.43	0.37
MgO	16.14	12.35	12.27	12.20	17.21	12.10	12.20	12.04	11.94	10.64	8.71
CaO	11.45	11.35	11.40	11.35	11.88	11.94	10.93	11.73	11.15	9.38	10.37
Na_2O	0.69	1.62	1.69	1.71	0.09	1.00	1.23	1.06	1.25	0.64	1.14
K_2O	0.28	0.86	0.91	0.92	0.03	0.69	0.71	0.81	0.79	0.24	0.58
C site											
Si	7.36	6.64	6.58	6.56	7.87	6.93	6.90	6.85	6.84	7.34	6.99
Al	0.64	1.36	1.43	1.44	0.11	1.07	1.10	1.15	1.17	0.52	1.01
Fe^{3+}	0.00	0.00	0.00	0.00	0.03	0.00	0.00	0.00	0.00	0.15	0.00
C site											
Al	0.09	0.20	0.16	0.18	0.00	0.12	0.07	0.08	0.00	0.00	0.03
Cr	0.00	0.01	0.01	0.01	0.00	0.00	0.01	0.00	0.00	0.00	0.00
Fe^3	0.78	0.47	0.47	0.44	0.49	0.47	0.80	0.54	0.75	1.44	1.05
Ti	0.03	0.24	0.26	0.27	0.01	0.15	0.16	0.19	0.19	0.03	0.07
Mg	3.41	2.71	2.70	2.70	3.62	2.65	2.66	2.64	2.62	2.31	1.95
Fe^{2+}	0.67	1.35	1.38	1.38	0.85	1.57	1.27	1.52	1.39	1.16	1.85
Mn	0.03	0.02	0.02	0.02	0.03	0.03	0.04	0.04	0.04	0.05	0.05
C site											
Ca	1.74	1.79	1.81	1.80	1.80	1.88	1.71	1.85	1.76	1.46	1.67
Na	0.19	0.21	0.20	0.20	0.03	0.12	0.29	0.15	0.24	0.18	0.33
C site											
Na	0.00	0.25	0.29	0.29	0.00	0.17	0.06	0.15	0.12	0.00	0.01
K	0.05	0.16	0.17	0.17	0.01	0.13	0.13	0.15	0.15	0.05	0.11
Sum cations	14.98	15.41	15.46	15.47	14.83	15.29	15.19	15.31	15.27	14.69	15.12
Fe#	0.30	0.40	0.41	0.40	0.27	0.43	0.44	0.44	0.45	0.54	0.60
Mg#	0.70	0.60	0.59	0.60	0.73	0.57	0.56	0.56	0.55	0.46	0.40

Mg/Md: monzogabbro/monzodiorite.

Table 3. (Continued).

Sample	7B.21	7B.22	7B.23	7B.31	7B.32	7B.33	7B.34	7B.41	7B.42	7B.43	7B.61
Location	Mg/Md	Mg/Md	Mg/Md	Mg/Md	Mg/Md	Mg/Md	Mg/Md	Mg/Md	Mg/Md	Mg/Md	Mg/Md
SiO_2	46.67	46.25	51.30	52.50	53.72	52.97	39.28	53.77	51.53	53.85	47.91
TiO_2	1.39	1.54	0.47	0.11	0.07	0.12	0.48	0.02	0.46	0.07	1.01
Al_2O_3	5.92	6.37	3.02	1.63	0.92	0.83	10.00	0.21	2.53	0.39	4.87
FeO	19.77	20.07	17.56	19.49	20.59	20.39	25.93	21.38	21.42	24.42	20.71
Cr_2O_3	0.00	0.00	0.03	0.00	0.00	0.00	0.00	0.02	0.00	0.01	0.05
MnO	0.26	0.24	0.26	0.34	0.25	0.38	0.21	0.26	0.36	0.66	0.32
MgO	10.57	10.28	12.95	11.13	11.28	11.20	5.27	10.22	10.57	12.16	10.16
CaO	10.79	10.65	11.28	11.81	10.99	11.23	10.80	11.55	10.92	6.79	10.91
Na_2O	1.49	1.52	0.81	0.16	0.05	0.10	1.57	0.03	0.45	0.03	1.19
K_2O	0.70	0.77	0.32	0.07	0.08	0.04	1.87	0.02	0.31	0.03	0.51
T site											
Si	6.96	6.89	7.46	7.78	7.84	7.82	6.29	8.00	7.54	7.49	7.14
Al	1.04	1.11	0.52	0.22	0.16	0.14	1.71	0.00	0.44	0.06	0.86
Fe^{3+}	0.00	0.00	0.03	0.00	0.00	0.04	0.00	0.00	0.02	0.45	0.00
C site											
Al	0.00	0.01	0.00	0.07	0.00	0.00	0.18	0.04	0.00	0.00	0.00
Cr	0.00	0.00	0.00	0.00	0.00	0.00	0.00	0.00	0.00	0.00	0.01
Fe^3	0.72	0.76	0.64	0.31	0.68	0.57	0.83	0.26	0.75	2.39	0.70
Ti	0.16	0.17	0.05	0.01	0.01	0.01	0.06	0.00	0.05	0.01	0.11
Mg	2.35	2.28	2.81	2.46	2.45	2.46	1.26	2.27	2.31	2.52	2.26
Fe^{2+}	1.74	1.74	1.47	2.11	1.83	1.91	2.64	2.40	1.85	0.00	1.89
Mn	0.03	0.03	0.03	0.04	0.03	0.05	0.03	0.03	0.05	0.08	0.04
B site											
Ca	1.72	1.70	1.76	1.88	1.72	1.78	1.85	1.84	1.71	1.01	1.74
Na	0.28	0.30	0.23	0.05	0.01	0.03	0.15	0.01	0.13	0.01	0.26
A site											
Na	0.15	0.14	0.00	0.00	0.00	0.00	0.34	0.00	0.00	0.00	0.09
K	0.13	0.15	0.06	0.01	0.02	0.01	0.38	0.00	0.06	0.01	0.10
Sum cations	15.29	15.29	15.04	14.94	14.75	14.81	15.72	14.85	14.90	14.03	15.18
Fe#	0.51	0.52	0.43	0.50	0.51	0.51	0.73	0.54	0.53	0.53	0.53
Mg#	0.49	0.48	0.57	0.50	0.49	0.49	0.27	0.46	0.47	0.47	0.47

Mg/Md: monzogabbro/monzodiorite.

Table 3. (Continued).

Sample	7B.62	7B.63	25A.1	25A.2	25A.3	1B.11	1B.12	1B.13	1B.21	1B.22	1B.23
Location	Mg/Md	Mg/Md	Syn	Syn	Syn	Syn	Syn	Syn	Syn	Syn	Syn
SiO_2	50.38	46.72	47.64	49.11	48.79	45.79	47.46	45.26	50.57	46.34	45.67
TiO_2	0.79	1.38	0.88	0.85	0.94	1.31	1.19	1.45	0.13	1.28	1.37
Al_2O_3	3.44	5.93	5.29	5.27	5.41	5.31	4.64	5.74	2.08	4.89	5.21
FeO	18.65	20.86	15.14	16.08	15.48	26.00	26.19	26.18	25.33	26.81	26.40
Cr_2O_3	0.05	0.00	0.00	0.00	0.00	0.00	0.02	0.00	0.00	0.02	0.03
MnO	0.31	0.27	0.65	0.69	0.59	0.78	0.84	0.67	0.88	0.92	0.82
MgO	11.90	9.90	13.17	13.27	13.57	6.57	7.03	6.12	7.36	6.55	6.28
CaO	11.09	10.55	11.59	11.03	10.74	9.52	9.38	9.67	10.55	9.09	9.62
Na_2O	0.75	1.43	1.14	1.07	1.11	1.63	1.37	1.53	0.49	1.50	1.58
K_2O	0.35	0.64	0.55	0.46	0.54	0.63	0.57	0.66	0.21	0.50	0.59
T site											
Si	7.39	6.97	7.09	7.11	7.08	6.98	7.10	6.95	7.64	7.00	6.99
Al	0.59	1.03	0.91	0.89	0.92	0.95	0.82	1.04	0.36	0.87	0.94
Fe^{3+}	0.02	0.00	0.00	0.00	0.00	0.06	0.09	0.02	0.00	0.13	0.08
C site											
Al	0.00	0.01	0.02	0.01	0.01	0.00	0.00	0.00	0.01	0.00	0.00
Cr	0.01	0.00	0.00	0.00	0.00	0.00	0.00	0.00	0.00	0.00	0.00
Fe^3	0.67	0.81	0.57	0.88	0.95	1.00	1.12	0.95	0.71	1.23	0.96
Ti	0.09	0.16	0.10	0.09	0.10	0.15	0.13	0.17	0.02	0.15	0.16
Mg	2.60	2.20	2.92	2.87	2.94	1.49	1.57	1.40	1.66	1.48	1.43
Fe^{2+}	1.60	1.79	1.31	1.06	0.93	2.26	2.07	2.39	2.49	2.03	2.34
Mn	0.04	0.03	0.08	0.09	0.07	0.10	0.11	0.09	0.11	0.12	0.11
B site											
Ca	1.74	1.69	1.85	1.71	1.67	1.56	1.50	1.59	1.71	1.47	1.58
Na	0.21	0.31	0.15	0.29	0.31	0.44	0.40	0.41	0.14	0.44	0.42
A site											
Na	0.00	0.10	0.18	0.01	0.00	0.04	0.00	0.05	0.00	0.00	0.05
K	0.07	0.12	0.10	0.09	0.10	0.12	0.11	0.13	0.04	0.10	0.12
Sum cations	15.02	15.22	15.28	15.10	15.08	15.16	15.01	15.18	14.89	15.01	15.16
Fe#	0.47	0.54	0.39	0.40	0.39	0.69	0.68	0.71	0.66	0.70	0.70
Mg#	0.53	0.46	0.61	0.60	0.61	0.31	0.32	0.29	0.34	0.30	0.30

Mg/Md: monzogabbro/monzodiorite; Syn: syenite.

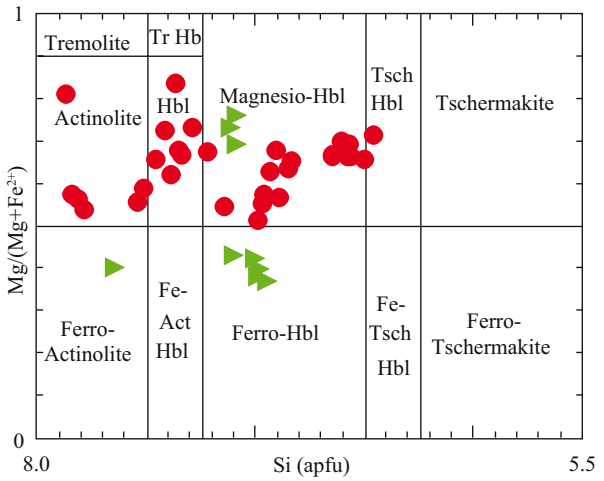

Figure 6. Classification of amphiboles according to the nomenclature of Leake et al. (1997); symbols as in Figure 2.

biotite + hornblende + titanite + magnetite or ilmenite) such that it clearly limits compositional influences (Leake and Said, 1994; Ague, 1997). In this paper, all selected samples have the above mineral assemblage, which is an important prerequisite for aluminum-in-hornblende barometry.

In addition, hornblende should have crystallized at approximately the same temperature close to the isothermal solidus and is not applicable to actinolite and actinolitic hornblende (Leake, 1971). Therefore, we have selected hornblende rims without actinolite and actinolitic hornblende compositions for this study (Figure 8a).

Oxygen fugacity has a marked effect on this mineral system and Anderson and Smith (1995) recommended just using amphiboles with a Fe# [Fe/(Mg + Fe)] value of <0.65 for barometric analyses. The selected amphiboles for barometry containing Fe# of <0.65 corresponding to Mg-hornblendes and iron-rich amphiboles are not appropriate for Al-in-hornblende geobarometry. Enami et al. (1993) stated that Fe# cannot stand as the only criterion for determining the oxygen fugacity and occurrence of euhedral titanite and magnetite as early-crystallizing phases indicate that the magma was relatively oxidized. In these samples, existence of euhedral titanite and magnetite along with other minerals indicates that the oxygen fugacity of the melt was relatively high.

Other prerequisites for a correct application of the barometers are as follows: the Si-activity of the melt must have been SiO_2-saturated (Si ≤7.5 apfu), because the Al-content of hornblende is directly related to its Si content; hornblendes with Ca ≥1.6 apfu (Hammarstrom and Zen, 1986; Bando, 2003); amphibole should coexist with quartz (Hammarstrom and Zen, 1986) and/or K-feldspar (Stein and Dietl, 2001), because its activity also influences the Al-content of hornblende; water saturation magmatic system (Anderson and Smith, 1995); and plagioclase coexisting with hornblende should range between An_{25} and An_{35} (Stein and Dietl, 2001).

All the analyses of amphiboles satisfy the criteria established (Si of ≤7.5 and Ca of ≥1.6 apfu) and measured rims of hornblende are in contact with quartz and/or K-feldspar, while the anorthite-contents in plagioclase are close to the true value within the defined limitations and also

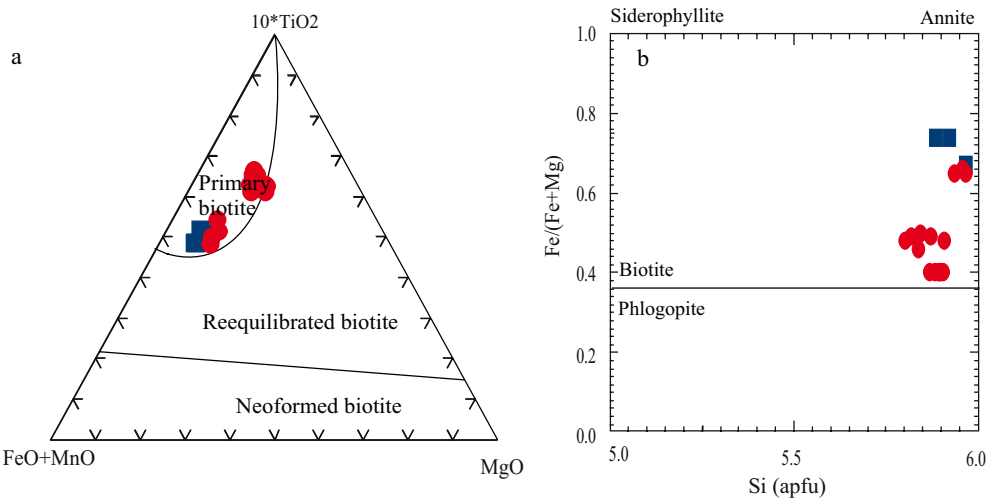

Figure 7. (a) Chemical composition of the South Dehgolan intrusion biotite crystals in the granite and monzodiorite rocks, using the 10^*TiO_2–FeO*–MgO ternary diagram discriminating among primary magmatic, reequilibrated, and neoformed biotites (Nachit et al., 2005); **(b)** classification of biotite analyses in the Si vs. Fe/(Fe + Mg) diagram symbols as in Figure 2.

Table 4. Electron microprobe analyses of biotite in the South Dehgolan intrusion.

Sample	18B.1	18B.2	18B.3	18B.4	7B.4.1	7B.4.2	7B.4.3	7B.4.4	14C.11.1	14C.11.2
Location	Gra	Gra	Gra	Gra	Mg/Md	Mg/Md	Mg/Md	Mg/Md	Mg/Md	Mg/Md
SiO_2	34.82	34.74	35.34	35.65	35.87	36.96	36.04	35.20	36.88	36.73
TiO_2	4.29	3.62	3.82	3.55	4.13	3.70	3.63	3.35	5.89	5.75
Al_2O_3	10.24	10.69	9.78	10.51	12.01	11.59	11.79	11.50	13.09	13.33
FeO	32.73	31.62	28.71	30.53	26.45	25.94	27.62	27.39	18.86	18.26
MnO	0.23	0.26	0.39	0.38	0.10	0.10	0.17	0.15	0.12	0.10
MgO	6.39	6.21	7.92	6.30	7.68	8.82	8.21	8.36	11.20	11.79
CaO	0.05	0.06	0.12	0.12	0.02	0.05	0.05	0.13	0.05	0.02
Na_2O	0.04	0.01	0.03	0.05	0.04	0.04	0.00	0.04	0.10	0.11
K_2O	7.32	7.94	9.74	8.24	8.73	8.65	7.84	7.72	9.24	9.28
Si	5.89	5.92	5.97	6.03	5.96	6.05	5.97	5.94	5.87	5.84
Al^{IV}	2.04	2.08	1.95	1.97	2.04	1.95	2.03	2.07	2.13	2.16
Al^{VI}	0.00	0.07	0.00	0.13	0.31	0.28	0.26	0.22	0.33	0.33
Ti	0.55	0.47	0.49	0.45	0.52	0.46	0.45	0.43	0.71	0.69
Fe^{2+}	4.63	4.51	4.05	4.32	3.67	3.55	3.82	3.86	2.51	2.43
Mn	0.03	0.04	0.06	0.06	0.01	0.01	0.02	0.02	0.02	0.01
Mg	1.61	1.58	1.99	1.59	1.90	2.15	2.03	2.10	2.66	2.79
Ba	0.00	0.00	0.00	0.00	0.00	0.00	0.00	0.00	0.00	0.00
Ca	0.01	0.01	0.02	0.02	0.00	0.01	0.01	0.02	0.01	0.00
Na	0.01	0.01	0.01	0.02	0.01	0.01	0.00	0.01	0.03	0.03
K	1.58	1.73	2.10	1.78	1.85	1.81	1.66	1.66	1.88	1.88
Sum cations	16.34	16.40	16.63	16.36	16.28	16.29	16.26	16.33	16.14	16.18
Fe#	0.74	0.74	0.67	0.73	0.66	0.62	0.65	0.65	0.49	0.46
Mg#	0.26	0.26	0.33	0.27	0.34	0.38	0.35	0.35	0.51	0.54

Mg/Md: monzogabbro/monzodiorite; Gra: granite.

Table 4. Continued.

Sample	14C.11.3	14C.22.1	14C.22.2	14C.22.3	8B.11.1	8B.11.2	8B.11.3	8B.22.1	8B.22.2	8B.22.3
Location	Mg/Md	Mg/Md	Mg/Md	Mg/Md	Mg/Md	Mg/Md	Mg/Md	Mg/Md	Mg/Md	Mg/Md
SiO_2	36.44	36.47	37.09	35.51	37.45	37.92	37.11	37.76	37.64	37.56
TiO_2	6.10	5.86	4.98	5.12	5.04	5.12	4.74	5.12	5.07	5.13
Al_2O_3	13.32	13.29	13.04	13.03	13.21	13.41	13.61	13.52	13.47	13.50
FeO	18.84	19.19	19.30	19.23	16.36	16.21	16.24	16.31	16.13	16.28
MnO	0.10	0.08	0.09	0.07	0.09	0.08	0.09	0.09	0.10	0.09
MgO	11.32	11.17	11.70	10.72	13.73	13.91	13.60	13.73	13.82	13.70
CaO	0.02	0.01	0.03	0.07	0.05	0.04	0.10	0.00	0.00	0.04
Na_2O	0.16	0.09	0.06	0.10	0.16	0.21	0.19	0.17	0.16	0.17
K_2O	9.22	9.33	9.25	8.89	8.88	9.06	8.97	9.17	9.09	9.10
Si	5.80	5.82	5.91	5.84	5.90	5.90	5.87	5.89	5.90	5.88
Al^{IV}	2.20	2.18	2.09	2.16	2.10	2.10	2.13	2.11	2.11	2.12
Al^{VI}	0.30	0.32	0.35	0.37	0.35	0.36	0.40	0.38	0.38	0.37
Ti	0.73	0.70	0.60	0.63	0.60	0.60	0.56	0.60	0.60	0.60
Fe^{2+}	2.51	2.56	2.57	2.65	2.16	2.11	2.15	2.13	2.11	2.13
Mn	0.01	0.01	0.01	0.01	0.01	0.01	0.01	0.01	0.01	0.01
Mg	2.69	2.66	2.78	2.63	3.22	3.23	3.21	3.20	3.23	3.20
Ba	0.00	0.00	0.00	0.00	0.00	0.00	0.00	0.00	0.00	0.00
Ca	0.00	0.00	0.01	0.01	0.01	0.01	0.02	0.00	0.00	0.01
Na	0.05	0.03	0.02	0.03	0.05	0.06	0.06	0.05	0.05	0.05
K	1.87	1.90	1.88	1.87	1.79	1.80	1.81	1.83	1.82	1.82
Sum cations	16.17	16.19	16.22	16.20	16.19	16.19	16.23	16.20	16.19	16.20
Fe#	0.48	0.49	0.48	0.50	0.40	0.40	0.40	0.40	0.40	0.40
Mg#	0.52	0.51	0.52	0.50	0.60	0.60	0.60	0.60	0.60	0.60

Mg/Md: monzogabbro/monzodiorite.

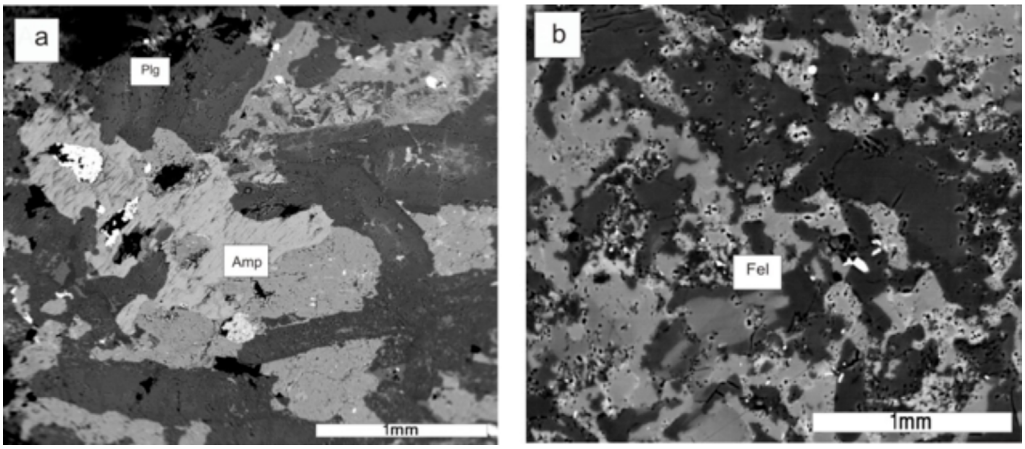

Figure 8. SEM backscattered electron images of **(a)** the amphibole coexisting with plagioclase in the monzogabbro-monzodiorite and **(b)** intergrowths of plagioclase and K-feldspar in the granite.

the magmatic system crystallized above the H_2O-saturated granite solidus; this is another important prerequisite for application of Al-in-hornblende barometry that was used to estimate the physicochemical parameters of magma crystallization in the studied intrusion. According to the calibration of Schmidt (1992), the average pressure estimates for monzogabbro-monzodiorite and syenite rocks are 1.9 and 1.3 ± 0.6 kbar, respectively (Table 5), for the final emplacement level and crystallization, indicating a shallow depth of emplacement of the studied rocks.

Anderson and Smith (1995) showed that the Al-content of hornblende is controlled not only by pressure but also by temperature. Because the influence of temperature on the pressure calculations has to be considered, the calibration of Anderson and Smith (1995) was chosen to calculate the crystallization pressures of the studied intrusion. The average pressures of crystallization of these samples from monzogabbro-monzodiorite and syenite rocks obtained from the Anderson and Smith (1995) calibration using revised temperature estimates with the correction of Vyhnal et al. (1991) are 1.6 and 1.3 ± 0.6 kbar, respectively (Table 5).

Pressures were calculated by the methods of Schmidt (1992) and were compared with results obtained from the Anderson and Smith (1995) calibration; slightly higher pressure estimates were obtained from the calibration of Schmidt (1992), but, considering errors, the estimated pressures correspond well with each other. The decrease in pressure from the monzogabbro-monzodiorite to syenite rocks suggests that the monzogabbro-monzodiorite was

Table 5. Results of barometry in the South Dehgolan intrusion according to method of 1) Schmidt (1992) and 2) Anderson and Smith (1995).

	7B1-2	7B2-1	7B2-2	1B-11	1B-12	1B-13	1B-22
Barometry	Mg/Md	Mg/Md	Mg/Md	Mg/Md	Mg/Md	Mg/Md	Mg/Md
Method 1	2.55	2.84	2.54	1.53	0.88	1.93	1.13
Method 2	2.10	2.28	2.10	1.40	0.87	1.69	1.08
	1B-23	7B-12	7B-21	7B-22	7B-61	7B-63	Average
Barometry	Mg/Md	Mg/Md	Mg/Md	Mg/Md	Mg/Md	Mg/Md	Mg/Md
Method 1	1.45	1.94	1.94	2.31	1.06	1.95	1.87
Method 2	1.34	1.70	1.70	1.95	1.02	1.71	1.62
	25A-1	25A-2	25A-3				
Barometry	Syn	Syn	Syn	Average			
Method 1	1.40	1.27	1.39	1.35			
Method 2	1.30	1.19	1.29	1.26			

Mg/Md: monzogabbro/monzodiorite; Syn: syenite.

crystallized earlier than the syenites at slightly greater depths consistent with other textural observations.

For granitic rocks, feldspar is the most useful mineral for geobarometry, because it is usually abundant in these rocks (Figure 8b). The crystallization pressure conditions of the granitic rocks have been estimated to be 1.9 kbar using the barometer of Putirka (2005) (see Table 6).

Likewise, a pressure range was obtained with the multivariate geothermometer of Soesoo (1997) using the X_{PT} vs. X_{PT} diagram (Figure 9a); the estimated pressures are in the range of 2–5 kbar and <2 kbar in monzogabbro-monzodiorite and syenite rocks, respectively. It can also be deduced that the pyroxene crystallization pressure of the monzogabbro-monzodiorite rocks was higher than for the syenite rocks. The highest pressure calculated is from clinopyroxene geobarometry, reflecting initial crystallization pressure of liquidus pyroxene from the differentially crystallizing magma.

Understanding the evolution of the intrusive rocks requires knowledge of the depth at which the intrusion crystallized. The calculated pressures obtained by Al-hornblende can represent conditions during final emplacement and determination of the intrusion depth. Intrusion depths were estimated assuming an average density of 2.65 g/cm^3 for the continental crust and from the average of all calculated pressures (lithostatic load). These pressure estimates indicate that the monzogabbro-monzodiorite, syenite, and granite rocks were emplaced at depths of about 6.7, 5.0, and 7.3 km, respectively. Although this geobarometry yields a crystallization pressure that is notably higher in the granite rocks compared to the other units, this difference is interpreted to be the result of differences in physical and chemical properties of the magma and/or different natures of these magmas (cf. Carmichael, 1991). The results are in good agreement with petrographic observations and textural evidence for high-level emplacements in the monzogabbro-monzodiorite, syenite, and granite rocks: medium- to fine-grained, granophyric textures, and sharp, angular contacts to uppermost crustal country rocks where exposed, i.e. like low-grade metamorphic aureole, hydrothermal alteration, and cognate volcanic rocks nearby (see Clarke, 1992).

In addition, crystallization depths of pyroxene in the monzogabbro-monzodiorite rocks range from 19 to 7 km and in the syenite rocks are <7 km, reflecting initial crystallization depth in the South Dehgolan intrusion.

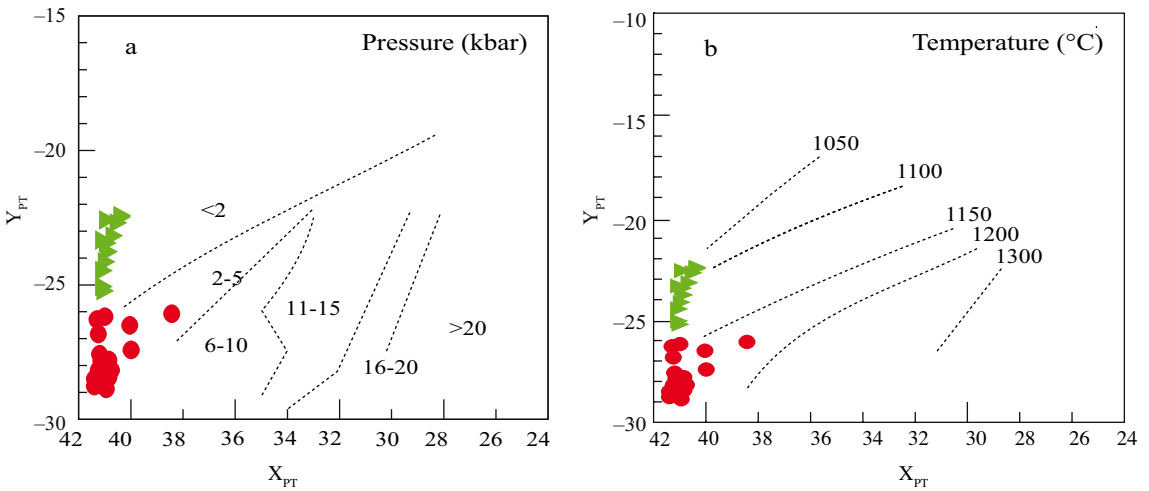

Figure 9. X_{PT} vs. Y_{PT} diagram (after Soesoo, 1997) of clinopyroxene composition in the estimation of **(a)** pressure and **(b)** temperature (X_{PT} = 0.446 SiO_2 + 0.187 TiO_2 – 0.404 Al_2O_3 + 0.346 FeO – 0.052 MnO + 0.309 MgO + 0.431 CaO – 0.466 Na_2O; Y_{PT} = –0.369 SiO_2 + 0.535 TiO_2 – 0.317 Al_2O_3 + 0.323 FeO + 0.235 MnO – 0.516 MgO – 0.167 CaO – 0.153 Na_2O); symbols as in Figure 2.

Table 6. Results of physicochemical conditions in the South Dehgolan intrusion according to the method of Putirka (2005, 2008).

	Putirka (2005)	Putirka (2005)	Putirka (2005)	Putirka (2008 (Eq. 24a))
	H_2O (wt. %)	P (kbar)	(1) T (°C)	(2) T (°C)
19A5.1 (granite)	3.8	1.9	789	762

Hornblende and plagioclase are commonly coexisting minerals in calc-alkaline igneous rocks, so they are usually used for thermometry (Blundy and Holland, 1990; Holland and Blundy, 1994; Stein and Dietl, 2001; Ernst, 2002). Holland and Blundy (1994) calibrated this thermometer and defined the following conditions for using it: temperature in the range of 400–900 °C; amphiboles that have ^{A}Na >0.02 pfu, Al^{VI} <1.8 pfu, and Si in the range of 6.0–7.7 pfu; and plagioclases with X_{an} <0.90. These compositional constraints in these amphiboles enable the use of this geothermometer. This geothermometer requires an estimate of pressure, so Schmidt's (1992) geobarometer was applied to estimate temperature and afterwards the revised pressure was calculated using the method of Anderson and Smith (1995). The hornblende-plagioclase geothermometer of Holland and Blundy (1994) is based on the edenite-richterite reaction and is applicable also to quartz-free igneous rocks; the average temperatures of equilibration calculated with the outer margin compositions of adjacent hornblende and plagioclase in the monzogabbro-monzodiorite rocks are 776 and 772 ± 40 °C and in the syenite rocks are 655 and 655 ± 40 °C using the geobarometers of Schmidt (1992) and of Anderson and Smith (1995), respectively (Table 7). The wide temperature range reflects changing solidification conditions in the studied intrusion. It is noteworthy that the pressures determined by either the Schmidt (1992) or the Anderson and Smith (1995) method for the estimation of temperature are similar, representing the reliable consolidation temperature of the body, and they can be indicative of solidus temperature, which is near the wet granodiorite solidus at 3 to 5 kbar (Whitney, 1988). As expected, the data also indicate that the monzogabbro-monzodiorite has higher temperatures than the syenitic rocks.

Similar results were also obtained for another method that was proposed by Ridolfi et al. (2010); using this geothermometry, amphiboles of certain samples displaying magnesiohornblende compositions with a calc-alkaline nature were selected and yielded average geothermometric estimates for the monzogabbro-monzodiorite rocks of 778 ± 57 °C using the Ridolfi et al. (2010) formula (Table 8). The estimated temperature corresponds well with the hornblende-plagioclase thermobarometry results.

The results also show that the pyroxene-bearing rocks were formed at higher temperatures than amphibole-containing ones. A decrease in temperature together with the evolution of these intrusions together with increasing silica content strongly suggests the influence of magma composition on crystallization temperatures, which may have been enhanced by the slow cooling of the adjacent mafic magmatic system.

Putirka (2005, 2008) proposed liquid-plagioclase geothermometry that can be used in granitic rocks. According to those proposed geothermometers (Putirka, 2005, 2008 (equation 24a); Table 6), the calculated average temperatures are 789 and 762 °C, respectively, indicating that it is higher than the syenitic rocks, indicating that they may be formed under different conditions.

The other geothermometers were used to estimate the crystallization temperature of pyroxenes. Using the X_{PT} vs. Y_{PT} diagram of Soesoo (1997), the clinopyroxenes of the studied monzogabbro-monzodiorite rocks were crystallized in the temperature range of 1150 to 1200 °C and in the syenite rocks between 1100 and 1150 °C (Figure 9b), assumed to reflect the actual temperature of initial pyroxene crystallization.

Furthermore, the clinopyroxene geothermometer of Bertrand and Mercier (1985, 1986; PT Mafic software) was used for temperature estimation as no orthopyroxene was observed to apply to the two-pyroxene geothermometer. On the basis of this geothermometer, crystallization

Table 7. Results of thermometry in the South Dehgolan intrusion according to method of Holland and Blundy (1994) and with barometers of 1) Anderson and Smith (1995) and 2) Schmidt (1992).

	7B	8B-1	8B-2	8B-3	8B-4	Average
T (Amp-Plg)	Mg/Md	Mg/Md	Mg/Md	Mg/Md	Mg/Md	Mg/Md
1	746	791	780	773.4	771	772
2	747	797	785	778	775	776
	25A-1	25A-2	25A-3	Average		
T (Amp-Plg)	Syn	Syn	Syn	Syn		
1	647	663	655	655		
2	647	663	655	655		

Mg/Md: monzogabbro/monzodiorite; Syn: syenite.

temperature was 1200–1370 °C in the monzogabbro-monzodiorite and 1100 °C in syenite rocks, which is a slightly higher temperature than that of the multivariate geothermometer of Soesoo (1997). These temperatures are usually higher than temperatures obtained by hornblende-plagioclase geothermometry. This suggests that the hornblende-plagioclase temperatures represent the late stage of magmatic crystallization of the South Dehgolan intrusion.

6.1.2. Estimation of oxygen fugacity (fO_2) and hygrometrics

The oxidation state of the magma can be monitored through mineral chemistry, Although it is difficult to estimate the original oxygen fugacities of primary magmas, as magnetite usually becomes Ti-free during slow cooling and ilmenite undergoes one or more stages of oxidation and exsolution (Haggerty, 1976), some inferences on the oxidation state of the magma can be made using the rock mineral assemblage and mineral composition.

Lalonde and Bernard (1993) correlated the color of biotite as observed in thin sections with concentrations of FeO, MgO, and TiO_2. They concluded that red biotites are Fe-rich, whereas the green or greenish brown biotites are Mg-rich, occurring more commonly in oxidized granitic rocks. Interestingly, the color of biotite is variable in the studied rocks, from dark brown to greenish in the monzogabbro-monzodiorite rocks and fox-red to brown in the granite rocks, reflecting differences in their redox conditions and a decrease in fO_2 in the granites (e.g., de Almedia et al., 2002). Ridolfi et al. (2010) proposed an empirical universal amphibole sensor to estimate of fO_2 parameters. According to Ridolfi et al. (2010), the values of log fO_2 calculated for monzogabbro-monzodiorite and syenite rocks are –13.3 and –13.5, respectively (maximum error: 0.41 log unit; Table 8).

When oxygen fugacity values are plotted on the log fO_2–T (°C) diagram (Wones and Eugster, 1965; Figure 10), the monzogabbro-monzodiorite samples follow a line parallel to the trend, above the NNO buffer and syenite rocks lie slightly higher than them, reflecting a relatively oxidizing condition. This is consistent with the presence of significant modal magnetite and euhedral titanite in the monzogabbro-monzodiorite and syenite of the studied intrusion that suggests crystallization at moderate to high fO_2. Therefore, the South Dehgolan intrusion is transitional, so that monzogabbro-monzodiorite and syenite rocks are formed in relatively oxidizing and granites formed in relatively reducing conditions.

Schweitzer (1979) proposed that the content of Fe^{3+} in pyroxenes depends on the fO_2 of melt, and hence it is shown on the Al^{IV} + Na vs. Al^{VI} + 2Ti + Cr diagram; samples of the monzogabbro-monzodiorite fall below and above the line of Fe^{3+} = 0, whereas the syenite rocks all fall above that line (Figure 11) and are relatively higher than monzogabbro-monzodiorite melt, in accordance with previous results. It seems that early-formed pyroxene crystallized under relatively reduced conditions, compared to those of other minerals.

A hygrometric formulation was also proposed by Ridolfi et al. (2010) using magnesiohornblende composition. According to the amphibole hygrometer of Ridolfi et al. (2010), the water contents in the monzogabbro-monzodiorite and syenite range from 4.7 to 4.4 wt.% (maximum error: 0.41 log unit; Table 8). The estimate of water contents in the initial granitic melts, based on Putirka (2005), is about 3.8 wt.% (Table 6) and is consistent with the results estimated from the model of Holtz et al. (2001, not shown), indicating that granite rocks contain less water in their initial melts compared to other units in the South Dehgolan intrusion.

Table 8. Results of physicochemical conditions in the South Dehgolan intrusion according to the method of Ridolfi et al. (2010).

	7B1-1	7B1-2	7B2-2	7B-21	Average
(Ridolfi et al., 2010)	Mg/Md	Mg/Md	Mg/Md	Mg/Md	Mg/Md
T (°C)	791	778	790	755	778
log fO_2	–13.2	–13.4	–13.3	–13.5	–13.3
H_2O_{melt} (wt.%)	5.3	4.8	4.3	4.3	4.7
	25A-1	25A-2	25A-3	Average	
(Ridolfi et al., 2010)	Syn	Syn	Syn	Syn	
log fO_2	–13.4	–13.8	–13.5	–13.5	
H_2O_{melt} (wt.%)	4.2	4.6	4.3	4.4	

Mg/Md: Monzogabbro/Monzodiorite; Syn: Syenite.

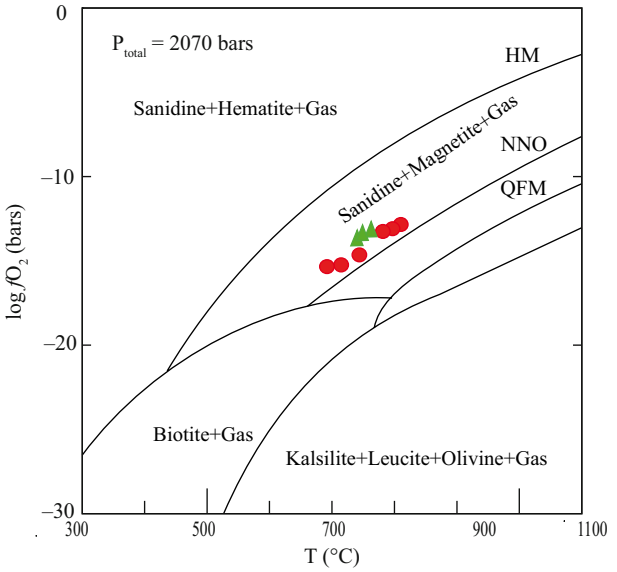

Figure 10. Temperature versus oxygen fugacity diagram (Wones and Eugster, 1965) as the solid lines show the fO_2–T (°C) conditions for buffers HM (hematite-magnetite), NNO (nickel-nickel oxide), and QFM (quartz-fayalite-magnetite); symbols as in Figure 2.

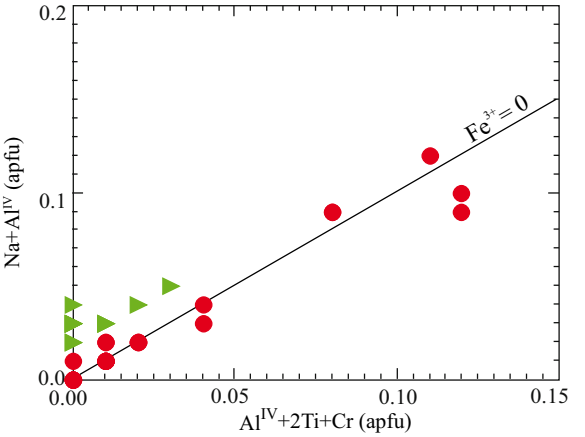

Figure 11. Na + Al^{IV} vs. Al^{IV} + 2Ti + Cr diagram (Schweitzer, 1979) of clinopyroxene composition in the estimation of oxygen fugacity; symbols as in Figure 2.

6.2. Nature of magma

In the present study, mineral compositions are considered as an effective tool for fingerprinting the magma type and potentially reflecting the nature of the magma in which they formed. In addition, mineral-chemical equilibria can help in delineating the tectonic environment of the South Dehgolan intrusion (e.g., Le Bas, 1962; Leterrier et al., 1982; Nachit, 1986; Abdel-Rahman, 1994; Molina et al., 2009). Other studies indicate that clinopyroxene compositions, in particular the minor element contents such as Ti, Al, Na, and Cr, as well as Si, are sensitive to magmatic affinities and geotectonic environments (Le Bas, 1962; Leterrier et al., 1982; Molina et al., 2009). Le Bas (1962) suggested that the incorporation of Si, Al, and Ti into the pyroxene lattice depends on the nature of the magma. According to Le Bas (1962), on the SiO_2 and TiO_2 vs. Al_2O_3 discrimination diagrams (Figure 12), the pyroxene from the South Dehgolan intrusion plot in the subalkaline and calc-alkaline fields indicates that they were formed in a subduction-related environment.

The compositions of amphibole from the South Dehgolan intrusion are mostly calcic, typical of I-type intrusions (Wyborn et al., 1981; White and Chappell, 1983; Clemens and Wall, 1984; Stein and Dietl, 2004).

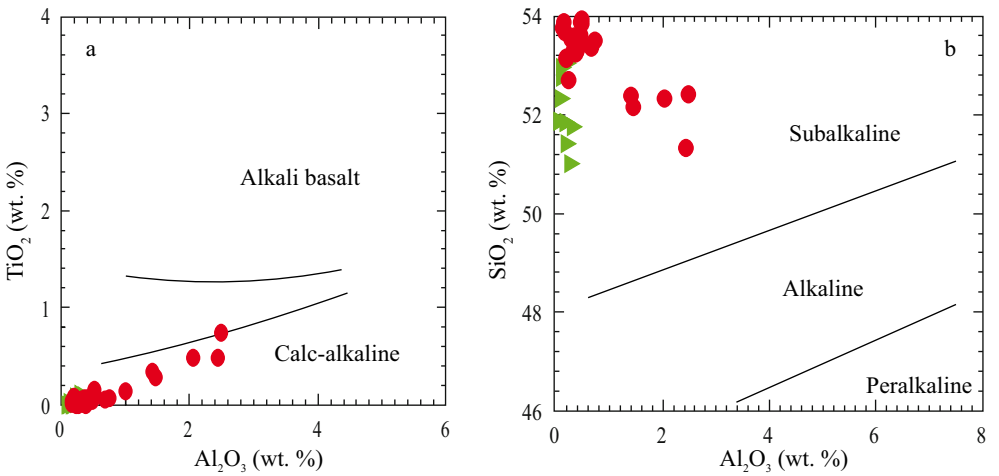

Figure 12. Composition of pyroxene on the Al_2O_3 (wt.%) vs. TiO_2 (wt.%) and SiO_2 (wt.%) binary diagrams (after Le Bas, 1962) used for discrimination of magmatic affinity and tectonic setting; symbols as in Figure 2.

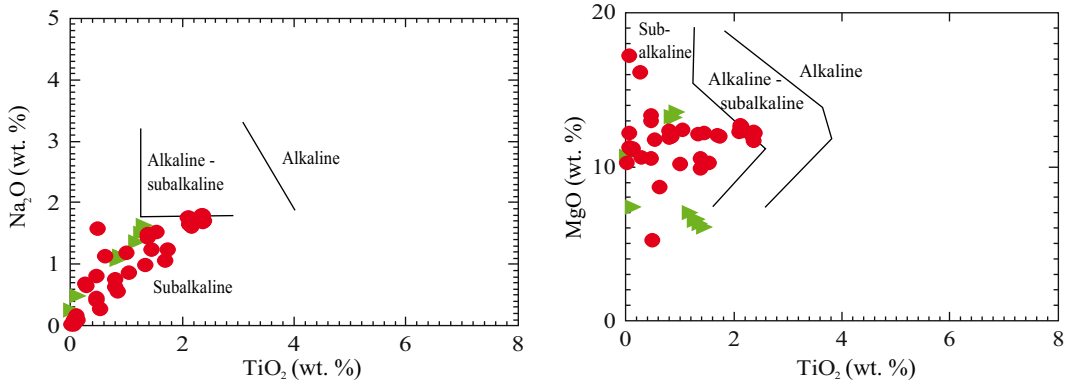

Figure 13. Na_2O (wt.%) and MgO (wt.%) vs. TiO_2 (wt.%) diagrams (Molina et al., 2009), discriminating the geochemical affinity and tectonic setting using amphibole composition; symbols as in Figure 2.

Molina et al. (2009) pointed out that amphiboles that crystallized from subalkaline melts usually have lower TiO_2, Al_2O_3, MgO, Na_2O, and K_2O contents and higher Na_2O/K_2O ratios than alkaline systems. As observed in Figure 13, amphiboles from monzogabbro-monzodiorite and syenite rocks fall in the subalkaline magmatic fields that are consistent with crystallization from I-type calc-alkaline granitoids.

According to Abdel-Rahman (1994), FeO/MgO ratios in biotite define three compositionally distinct fields: 1) biotites from alkaline anorogenic suites that are iron-rich siliceous annites and formed in association with extensional tectonic environments, with mean FeO/MgO = 7.04; 2) biotites from the peraluminous S-type granitoids that are siderophyllite with average FeO/MgO ratio = 3.48; and 3) biotites from the I-type calc-alkaline granitoids, typically formed within subduction-related environments and moderately enriched in Mg, with average FeO/MgO ratio of 1.76. Biotites of monzogabbro-monzodiorite rocks show FeO/MgO ratios in the 1.2–3.3 range (average = 1.88), whereas the FeO/MgO ratios of biotite analyzed from granites are moderately enriched in Fe, showing FeO/MgO ratios ranging from 3.6 to 5.1; these values are slightly higher than those proposed by Abdel-Rahman (1994) for biotites from calc-alkaline granitoids and lower than the biotites from alkaline anorogenic suites; these are similar to biotite compositions in the Queimadas Pluton that are proposed as A-type granites (de Almedia et al., 2002). In the MgO-FeO-Al_2O_3 discrimination diagram (Abdel-Rahman, 1994), most biotites from the monzogabbro-monzodiorite rocks fall within the calc-alkaline field and some monzodiorite samples and all granites samples plot in the alkaline suite field, representing A-type (Figure 14a) with high FeO relative to MgO and Al_2O_3. Shabani et al.

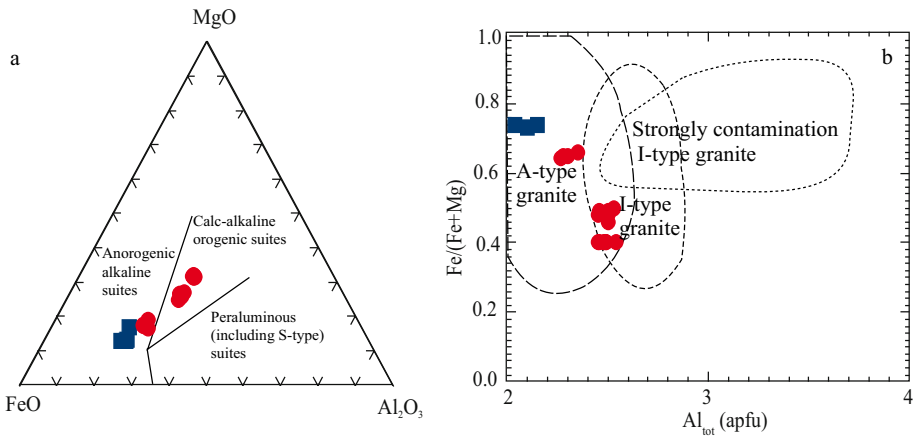

Figure 14. (a) Al_2O_3-FeO-MgO (Abdel-Rahman, 1994) and **(b)** Al vs. Fe/(Fe + Mg) (Shabani et al., 2003) biotite composition discrimination diagrams for distinguishing the nature of the studied granite and monzodiorite rocks; symbols as in Figure 2.

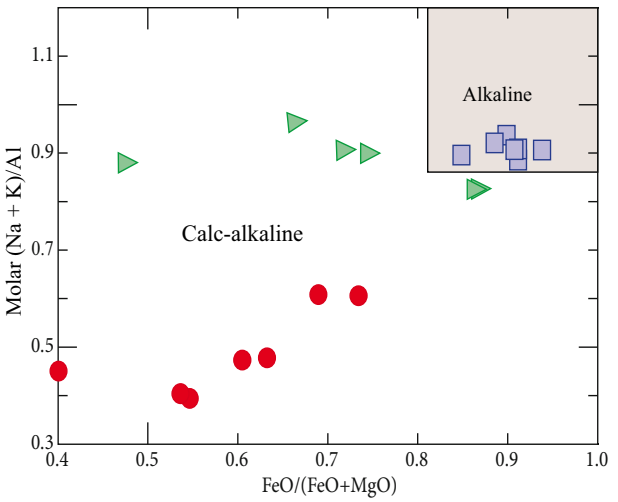

Figure 15. Agpaitic index (molar (Na + K)/Al) vs. FeO/(FeO + MgO) (Nardi, 1991) indicating calc-alkaline nature of monzogabbro-monzodiorite and syenite rocks and alkaline affinity of granite rocks.

(2003) dealt with a large database of biotite in granitoids from the Canadian Appalachians and obtained a similar result to the biotite geochemical discrimination diagrams of Abdel-Rahman (1994) (see Figure 14b). The studied samples plot in the I-type and A-type granite fields in the Al vs. Fe/(Fe + Mg) diagram (see Shabani et al., 2003), in accordance with previous results. The observations noted above are consistent with a change from calc-alkaline to alkaline nature, formed within a subduction-related environment.

Similar results were obtained using whole-rock chemical data (Table 9). The agpaitic index (AI; molar (Na+K/Al)) clearly separates the alkaline group with AI of >0.87 from calc-alkaline AI of <0.87. According to the geochemical classification of Nardi (1991; Figure 15), monzogabbro-monzodiorite and syenite rocks are calc-alkaline, but granites are alkaline, supporting the results of the biotite compositional systematics. This is consistent with the general idea that the Sanandaj-Sirjan zone is an ancient continentally situated convergent margin. The alkaline nature in some rocks can be attributed to a change in the geodynamic regime from compression to transtensional in the Sanandaj-Sirjan zone during subduction of the Neotethys oceanic crust beneath the Central Iranian microcontinent; a similar interpretation has been suggested by many workers who have pointed out

Table 9. The result of major element geochemical data from the South Dehgolan intrusion.

Sample	type	SiO_2	TiO_2	Al_2O_3	Fe_2O_3	FeO	MnO	MgO	CaO	Na_2O	K_2O	P_2O_5
R27	Mg/Md	52.1	0.83	19.7	1.32	2.1	0.11	4.94	11	4.43	1.47	0.08
R7B	Mg/Md	55.9	1.45	16.1	3.58	5.17	0.17	3.05	5.94	4.76	1.78	0.32
R11B	Mg/Md	50.3	1.54	15.7	3.48	6.23	0.18	5.46	7.93	3.62	1.43	0.31
R14	Mg/Md	50.5	1.7	16.2	3.32	5.86	0.17	5.8	9.04	3.72	1.43	0.27
M8B	Mg/Md	48.5	1.4	17	2.84	5.41	0.16	6.63	9.42	3.01	1.62	0.27
M6B	Mg/Md	51	0.95	16.6	2.76	5.24	0.15	6.7	8.94	3.25	1.26	0.07
R21B	Mg/Md	51.8	1.31	15.5	3.95	5.8	0.12	4.23	7.15	3.89	2.77	0.38
R26	Syn	64.5	1.02	16.3	1.18	1.16	0.05	1.12	3.75	9.45	0.06	0.21
M24B	Syn	63	1.1	15.9	1.66	1.57	0.1	1.04	4.18	5.96	4.01	0.22
R01	Syn	61	1.14	15.5	3.76	4.11	0.14	1.12	3.15	5.73	3.02	0.32
M1B	Syn	62.8	0.86	16.4	2.96	3.17	0.12	0.91	2.52	6.86	1.97	0.22
R30	Syn	59.8	1.24	16.3	1.31	1.41	0.06	2.84	7.59	8.09	0.88	0.26
24B	Syn	63.1	1.1	15.4	1.77	1.67	0.08	1.27	5.17	5.4	4.58	0.25
R05	Gra	77.6	0.06	11.5	0.37	0.38	0.01	0.08	0.11	2.97	5.44	0.01
M6B	Gra	75.1	0.16	12.3	0.6	0.61	0.01	0.15	0.16	3.62	4.96	0.01
R17	Gra	72.1	0.23	13.3	1.26	1.23	0.02	0.23	0.2	3.38	5.74	0.02
D5	Gra	72.3	0.28	13.9	1.54	1.39	0.03	0.27	0.21	3.5	6.38	0.04
16A	Gra	72.9	0.38	14.2	1.05	1.17	0.04	0.38	1.78	7.39	0.51	0.05
11B	Gra	75.8	0.21	13.2	0.73	0.7	0.02	0.09	0.14	3.98	5.02	0.03
19B	Gra	73.5	0.2	13.8	1.22	1.15	0.04	0.23	0.34	4.11	5.28	0.03

Mg/Md: monzogabbro/monzodiorite; Syn: syenite; Gra: granite.

that arc-related magmatic activity within the Sanandaj-Sirjan zone took place in an extensional geodynamic setting (e.g., Sawkins, 1984; Alavi, 1994; Tosdal and Richards, 2001; Mohajjel et al., 2003; Agard et al., 2005; Hassanzadeh et al., 2008).

Acknowledgments
Thanks to the University of Tehran, University of Kurdistan, and University of Payame Noor for supporting this project. We acknowledge F. Yavuz, E. Aldanmaz, Y. Eyüboğlu, and the anonymous reviewers for their constructive comments leading to important improvements in the manuscript.

References

Abdel-Rahman AM (1994). Nature of biotites from alkaline, calc-alkaline and peraluminous magmas. J Petrol 35: 525–541.

Agard P, Omrani J, Jolivet L, Mouthereau F (2005). Convergence history across Zagros (Iran): constraints from collisional and earlier deformation. Int J Earth Sci 94: 401–419.

Agemar T, Worner G, Heumann A (1997). Stable isotopes and amphibole chemistry on hydrothermally altered granitoids in the North Chilean Precordillera: a limited role for meteoric water? Contrib Mineral Petr 136: 331–344.

Ague JJ (1997). Thermodynamic calculation of emplacement pressures for batholithic rocks, California: implications for the aluminum-in-hornblende barometer. Geology 25: 563–566.

Alavi M (1994). Tectonics of Zagros orogenic belt of Iran: new data and interpretation. Tectonophysics 229: 211–238.

Alavi M (2004). Regional stratigraphy of the Zagros fold-thrust belt of Iran and its proforeland evolution. Am J Sci 304: 1–20.

Anderson JL (1996). Status of thermo-barometry in granitic batholiths. Earth Sci Rev 87: 125–138.

Anderson JL, Smith DR (1995). The effects of temperature and fO_2 on the Al-in-hornblende barometer. Am Mineral 80: 549–559.

Azizi H, Asahara Y, Mehrabi B, Chung SL (2011). Geochronological and geochemical constraints on the petrogenesis of high-K granite from the Suffi abad area, Sanandaj-Sirjan Zone, NW Iran. Chem Erde Geochem 71: 363–376.

Bando M, Bignall G, Sekine K, Tsuchiya N (2003). Petrography and uplift history of the Quaternary Takidani Granodiorite: could it have hosted a supercritical (HDR) geothermal reservoir? J Volcanol Geoth Res 120: 215–234.

Bertrand P, Mercier JCC (1985). The mutual solubility of coexisting ortho- and clinopyroxene: toward an absolute geothermometer for natural system? Earth Planet Sci Lett 76: 109–122.

Blundy JD, Holland TJB (1990). Calcic amphibole equilibria and a new amphibole- plagioclase geothermometer. Contrib Mineral Petr 104: 208–224.

Botcharnikov RE, Koepke J, Holtz F, McCammon C, Wilke M (2005). The effect of water activity on the oxidation and structural state of Fe in a ferro-basaltic melt. Geochim Cosmochim Ac 69: 5071–5085.

Carmichael ISE (1991). The redox state of basic and silicic magmas: a reflection of their source regions? Contrib Mineral Petr 106: 129–141.

Chivas AR (1981). Geochemical evidence for magmatic fluids in porphyry copper mineralization. Contrib Mineral Petr 78: 389–403.

Clarke DB (1992). Granitoid Rocks. London, UK: Chapman and Hall.

Clemens JD, Wall VJ (1984). Origin and evolution of a peraluminous silicic ignimbrite suite: the Violet Town Volcanics. Contrib Mineral Petr 88: 354–371.

Davi M, De Rosa R, Barca DA (2009). LA-ICP-MS study of minerals in the Rocche Rosse magmatic enclaves: evidence of a mafic input triggering the latest silicic eruption of Lipari Island (Aeolian Arc, Italy). J Volcanol Geoth Res 182: 45–56.

de Almedia CN, Guimaraes IP, da Silva Filho AF (2002). A-Type post-collisional granites in the Borborema Province, NE Brazil: the Queimadas Pluton. Gondwana Res 5: 667–681.

Deer WA, Howie RA, Zussman J (1992). An Introduction to the Rock-Forming Minerals. Essex, UK: Longman.

Droop GTR (1987). A general equation for estimating Fe^{3+} in ferromagnesian silicates and oxides from microprobe analysis, using stoichiometric criteria. Mineral Mag 51: 431–437.

Elliott BA, Ramo OT, Nironen M (1998). Mineral chemistry constraints on the evolution of the 1.88–1.87 Ga post-kinematic granite plutons in the Central Finland Granitoid Complex. Lithos 45: 109–129.

Enami M, Suzuki K, Liou JG, Bird DK (1993). Al–Fe^{3+} and F–OH substitutions in titanite and constrains on their P–T dependence. Eur J Mineral 5: 231–291.

Ernst WG (2002). Paragenesis and thermobarometry of Ca-amphiboles in the Barcroft granodioritic pluton, central White Mountains, eastern California. Am Mineral 87: 478–490.

Haggerty SE (1976). Opaque mineral oxides in terrestrial igneous rocks. Mineral Soc Am Short Course Notes 3: 101–300.

Hammarstrom JM, Zen E (1986). Aluminum in hornblende: an empirical igneous geobarometer. Am Mineral 71: 1297–1313.

Hassanzadeh J, Stockli DF, Horton BK, Axen GJ, Stockli LD, Grove M, Schmitt AK, Hempton MR (1987). Constraints on Arabian plate motion and extensional history of the Red Sea. Tectonics 6: 687–705.

Hendry DAF, Chivas AR, Long JVP, Reed SJB (1985). Chemical differences between minerals from mineralizing and barren intrusions from some North American porphyry copper deposits. Contrib Mineral Petr 89: 317–329.

Holland T, Blundy J (1994). Non-ideal interactions in calcic-amphiboles and their bearing on amphibole-plagioclase thermometry. Contrib Mineral Petr 116: 433–447.

Holton T, Jamtveit B, Meakin P (1999). Noise and oscillatory zoning of minerals. Geochim Cosmochim Ac 64: 1893–1904.

Holtz F, Johannes W, Tamic N, Behrens H (2001). Maximum and minimum water contents of granitic melts generated in the crust: a reevaluation and implications. Lithos 56: 1–14.

Jayasuriya KD, O'Neill HSC, Berry AJ, Campbell SJ (2004). A Mössbauer study of the oxidation state of Fe in silicate melts. Am Mineral 89: 1597–1609.

Kilinc A, Carmichael ISE, Rivers ML, Sack RO (1983). The ferric-ferrous ratio of natural silicate liquids equilibrated in air. Contrib Mineral Petr 83: 136–140.

Kress VC, Carmichael ISE (1991). The compressibility of silicate liquids containing Fe_2O_3 and the effect of composition, temperature, oxygen fugacity and pressure on their redox states. Contrib Mineral Petr 108: 82–92.

Lalonde AE, Bernard P (1993). Composition and color of biotite from granites: two useful properties in the characterization of plutonic suites from the Hepburn internal zone of Wopmay orogen, Northwest Territories. Can Mineral 31: 203–217.

Leake BE (1971). On aluminous and edenitic amphiboles. Mineral Mag 38: 389–407.

Leake BE (1978). Nomenclature of amphiboles. Am Mineral 63: 1023–1052.

Leake BE, Said YA (1994). Hornblende barometry of the Galway batholith, Ireland: an empirical test. Miner Petrol 51: 243–50.

Leake BE, Woolly AR, Arps CES, Birch WD, Gilbert MC, Grice JD, Hawthorne FC, Kato A, Kisch HJ, Krivovichev VG et al. (1997). Nomenclature of Amphiboles. Report of the Subcommittee on Amphiboles of the International Mineralogical Association Commission on New Minerals Names. Eur J Mineral 9: 623–651.

Le Bas MJ (1962). The role of aluminum in igneous clinopyroxenes with relation to their parentage. Am J Sci 260: 267–288.

Leterrier J, Maury RC, Thonon P, Girard D, Marchal M (1982). Clinopyroxene composition as a method of identification of the magmatic affinities of Paleo-volcanic series. Earth Planet Sci Lett 59: 139–154.

Mohajjel M, Fergusson CL (2000). Dextral transpression in Late Cretaceous continental collision Sanandaj–Sirjan zone western Iran. J Struct Geol 22: 1125–1139.

Mohajjel M, Fergusson CL, Sahandi MR (2003). Cretaceous-Tertiary convergence and continental collision, Sanandaj-Sirjan Zone, western Iran. J Asian Earth Sci 21: 397–412.

Molina J, Scarrow J, Montero PG, Bea F (2009). High-Ti amphibole as a petrogenetic indicator of magma chemistry: evidence for mildly alkalic-hybrid melts during evolution of Variscan basic–ultrabasic magmatism of Central Iberia. Contrib Mineral Petr 158: 69–98.

Morimoto N, Fabries J, Ferguson AK, Ginzburg IV, Ross M, Seifert FA, Zussman J, Aoki K, Gottardi G (1988). Nomenclature of pyroxenes. Am Mineral 73: 1123–1133.

Nachit H (1986). Contribution a letude analytique et experimental des biotite des granitoids Applications typologiques. PhD, University of Western Brittany, Brest, France (in French).

Nachit H, Ibhi A, Abia EH, Ohoud MB (2005). Discrimination between primary magmatic biotites, re-equilibrated biotites and neoformed biotites. CR Geosci 337: 1415–1420.

Nardi LVS (1991). Caracterização petrográfica e geoquímica dos granitos metaluminosos da associação alcalina: revisão. Pesquisas 18: 44–57 (in Portuguese).

Ottonello G, Moretti R, Marini L, Zuccolini MV (2001). Oxidation state of iron in silicate glasses and melts: a thermochemical model. Chem Geol 174: 157–179.

Pouchou JL, Pichoir F (1985). "PAP" (ρz) correction procedure for improved quantitative microanalysis. In: Armstrong JT, editor. Microbeam Analysis. San Francisco Press, San Francisco, CA, USA, pp. 104–106.

Putirka KD (2005). Igneous thermometers and barometers based on plagioclase + liquid equilibria: Tests of some existing models and new calibrations. Am Mineral 90: 336–346.

Putirka KD (2008). Introduction to minerals, inclusions and volcanic processes. Rev Mineral Geochem 69: 1–8.

Richard LR (1995). MinPet: Mineralogical and Petrological Data Processing System, Version 2.02. Gatineau, QC, Canada: MinPet Geological Software.

Ridolfi F, Renzulli A, Puerini M (2010). Stability and chemical equilibrium of amphibole in calc-alkaline magmas: an overview, new thermobarometric formulations and application to subduction-related volcanoes. Contrib Mineral Petr 160: 45–66.

Rieder M, Cavazzini G, D'yakonov YS, Frank-Kamenetskii VA, Gottardi G, Guggenheim S, Koval PV, Muller G, Neiva AMR, Radoslovich EW et al. (1999). Nomenclature of the micas. Mineral Mag 63: 267–279.

Robinson P, Spear FS, Schumacher JC, Laird J, Klein C, Evans BW, Doolan BL (1982). Phase relations of metamorphic amphiboles: natural occurrence and theory. Rev Mineral 9B: 1–228.

Rutter MJ, Van der laan SR, Wyllie PJ (1989). Experimental data for a proposed empirical igneous geobarometer: aluminium in hornblende at 10 kbar pressure. Geology 17: 897–900.

Sawkins EJ (1984). Metal Deposits in Relation to Plate Tectonics. Berlin, Germany: Springer.

Schmidt MW (1992). Amphibole composition in tonalite as a function of pressure an experimental calibration of the Al-hornblende barometer. Contrib Mineral Petr 110: 304–310.

Schweitzer EL, Papike JJ, Bence AE (1979). Statistical analysis of clinopyroxenes from deep-sea basalts. Am Mineral 64: 501–513.

Shabani AT, Lalonde AE, Whalen JB (2003). Composition of biotite from granite rocks of the Canadian Appalachian orogen: a potential tectonomagmatic indicator. Can Mineral 41: 1381–1396.

Soesoo A (1997). A multivariate statistical analysis of clinopyroxene composition: empirical coordinates for the crystallisation PT-estimations. Geol Soc Sweden (Geologiska Föreningen) 119: 55–60.

Stein E, Dietl E (2001). Hornblende thermobarometry of granitoids from the Central Odenwald (Germany) and their implication for the geotectonic development of the Odenwald. Miner Petrol 72: 185–207.

Streckeisen AL (1976). To each plutonic rock its proper name. Earth Sci Rev 12: 1–33.

Tosdal RM, Richards JP (2001). Magmatic and structural controls on the development of porphyry Cu ± Mo ± Au deposits. Rev Econ Geol 14: 157–181.

Vyhnal CR, McSween HY Jr, Speer JA (1991). Hornblende chemistry in southern Appalachian granitoids: implications for aluminum hornblende thermobarometry and magmatic epidote stability. Am Mineral 76: 176–188.

White AJR, Chappell BW (1983). Granitoid types and their distribution in the Lachlan Fold Belt, southeastern Australia. Geol Soc Am Mem 159: 21–34.

Whitney JA (1988). The origin of granite: the role and source of water in the evolution of granitic magmas. Geol Soc Am Bull 100: 1886–1897.

Wones DR, Eugster HP (1965). Stability of biotite: experiment, theory, and application. Am Mineral 50: 1228-1272.

Wyborn D, Chappell BW, Johnston RM (1981). Three S type volcanic suites from the Lachlan Fold Belt. Southeast Australia. J Geophys Res 86: 10335–10348.

Yang XM, Lentz DR (2005). Chemical composition of rock-forming minerals in gold-related granitoid intrusions, southwestern New Brunswick, Canada: implications for crystallization conditions, volatile exsolution, and fluorine-chlorine activity. Contrib Mineral Petr 150: 287–305.

Zahedi M, Hajian J, Blourchi H (1985). Geology Map of Sanandaj (Scale 1:250000). Tehran, Iran: Geology Survey.